SGG SGS sc | nat
Swiss Journal of Geosciences

ORIGINAL PAPER Open Access

Geochronology, geochemistry, and geological evolution of the Troiseck-Floning and Rosskogel nappes (Eastern Alps): unraveling parallels between the Eastern Alps and Western Carpathians

Martin K. Reiser[1*], Ralf Schuster[1], Christoph Iglseder[1], Daniela Gallhofer[2] and Josef Nievoll[3]

Abstract

The Troiseck-Floning and Rosskogel nappes are part of the Austroalpine Unit in the eastern part of the Eastern Alps. The nappes are in tectonic contact and comprise Permian to Mesozoic lower greenschist facies metamorphic metasediments, but only the Troiseck-Floning Nappe consists of a pre-Permian crystalline basement (Troiseck Complex) as well. LA-ICP-MS U–Pb zircon ages, Rb–Sr biotite ages and geochemical data unravel the geological evolution of these tectonic units from Neoproterozoic to Mesozoic times. Detrital U–Pb zircon analyses from siliciclastic metasediments of the Troiseck Complex indicate a late Ediacaran to early Cambrian deposition age of the volcanoclastic sequence. The age distribution correlates with a position along the northeastern Gondwana margin. A late Cambrian crystallization age (502.4 ± 6.8 Ma) of granitic intrusions together with evidence for Late Cambrian/Ordovician magmatism and metamorphism indicate a position at an active plate margin. Polyphase overprinting during the Variscan orogeny is recorded by Late Devonian/early Carboniferous pegmatite dikes (~ 353 Ma) that formed after an early Variscan event, while Pennsylvanian ages of overgrowth rims and inherited grains (~ 320 Ma) are evidence for late Variscan metamorphism. Rhyolitic to andesitic volcanic rocks from the Troiseck-Floning and Rosskogel nappes (271–264 Ma) concomitant with intrusions of porphyric granitoids now transformed to augen gneiss (271 Ma) yield evidence for Permian rift-related magmatism that is widely reported from the Eastern Alps and Western Carpathians. Rb–Sr biotite ages (75–74 Ma) indicate Late Cretaceous cooling below c. 300 °C. This relates to Late Cretaceous exhumation of the Troiseck-Floning Nappe following an Eo-Alpine metamorphic overprint at lower greenschist-facies metamorphic conditions. Based on the similar lithostratigraphy, analogous geological evolution and structure, the Troiseck-Floning Nappe represents the lateral extension of the Seckau Nappe. The new dataset also allows for correlations with other basement complexes that occur in the Western Carpathians.

Keywords Eastern Alps, Austroalpine, Silvretta-Seckau Nappe System, Geochemistry, Zircon U–Pb dating, Biotite Rb–Sr, Western Carpathians

Editorial handling: Marko Vrabec

*Correspondence:
Martin K. Reiser
martin.reiser@geosphere.at
Full list of author information is available at the end of the article

1 Introduction

The easternmost part of the Alpine orogen presents itself as an intricate arrangement of various pre-Alpine basement complexes and their respective Mesozoic cover sequences (Fig. 1). This juxtaposition of different crustal levels is the result of nappe stacking, exhumation and brittle deformation during the Alpine orogeny. Based on their Alpine overprint and palaeogeographic context, the tectonic interpretation of Schmid et al. (2004) and Froitzheim et al. (2008) subdivide the basement exposures into nappes and nappe systems of Upper and Lower Austroalpine affiliation. Unraveling the evolution of each of these basement complexes by their magmatic inventory and their structural and metamorphic overprints is essential for palaeogeographic reconstructions and correlations of the individual tectonic elements of the Alpine nappe stack.

Recently, new geochronological and geochemical data from the central and eastern parts of the Silvretta-Seckau Nappe System have shed new light on the magmatic and metamorphic history of the region. These data have been obtained from various complexes, including

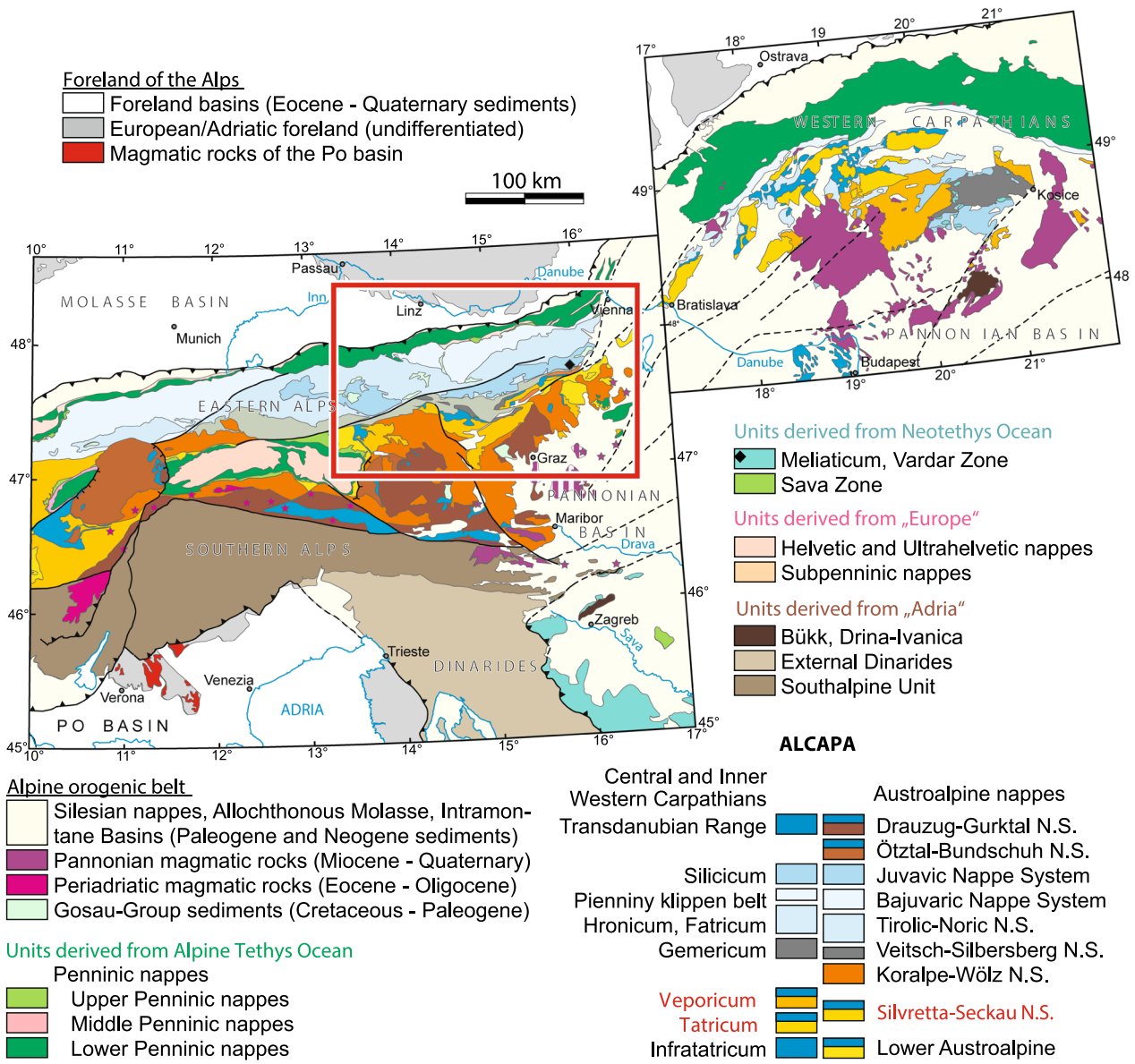

Fig. 1 Tectonic map of the Eastern Alps and Western Carpathians using the subdivision of Froitzheim et al. (2008). Additionally, the paleogeographic origin and a correlation of the ALCAPA-derived units is indicated. Abbreviation "N.S." in the legend stands for Nappe System. The red square refers to the area visualized in Fig. 2

the Golling- and Riesach Complex (Weißpriach, Duisitz and Obertal nappes; Huang et al., 2021; 2022), Seckau Complex (Seckau Nappe; Pfingstl et al., 2015; Mandl et al., 2018; 2022), and Waldbach Complex (Vorau Nappe; Chang et al., 2021). Nevertheless, there is still a significant data gap in the eastern part of the Silvretta-Seckau Nappe System concerning the Troiseck-Floning Nappe. The latter presumably represents the eastern continuation of the Seckau Nappe, separated by sinistral displacement along the Trofaiach Fault. However, the pre-Miocene relationship between the pre-Alpine basement complexes remains unclear due to a lack of protolith ages and an enigmatic pre-Alpine geological evolution of the Troiseck Complex.

This paper presents new geochronological and geochemical analyses of the Troiseck Complex, aiming to unravel its geological evolution, also in the context of neighboring units of the Silvretta-Seckau Nappe System. There is a general agreement on the correlation of the Eastern Alps and the Western Carpathians below the Vienna basin (e.g. Plašienka, 2018) and recent correlations focused on structural data (Tari et al., 2021) and the Cretaceous sedimentary cover of basement units (Hók et al., 2022). This study presents new data, which foster the correlation between the basement complexes. Altogether, the data presented contribute to the broader understanding of the Alpine-Carpathians orogen and its geological history.

2 Geological setting

The study focuses on the Troiseck-Floning Nappe of the Silvretta-Seckau Nappe System, representing the lowermost Upper Austroalpine tectonic unit in the Eastern Alps. Additionally, two samples from the directly underlying Rosskogel Nappe, traditionally attributed to the Lower Austroalpine unit were analyzed (Figs. 1, 2).

2.1 Troiseck-Floning Nappe

The Upper Austroalpine Troiseck-Floning Nappe extends about 70 km in WSW-ENE direction in northeastern Styria (Austria), from the area of Trofaiach in the West to Mürzzuschlag in the East. A pre-Variscan basement (the so-called Troiseck Complex; Schuster & Nowotny, 2016) and its Permian to Triassic cover sequence constitute the Troiseck-Floning Nappe (Fig. 3). The crystalline basement is composed of siliciclastic metasediments (paragneiss and micaschist), metabasites (amphibolite) and subordinate carbonatic layers (impure marble). The Troiseck Complex is permeated by lenses of deformed granitic igneous rocks and unconformably overlain by rhyolitic metavolcanics that constitute the base of Permian to Mesozoic sediments. The latter include Permian clastic sediments, Lower Triassic quartzite (Semmering quartzite) and Lower to Middle Triassic calcite marble, dolomite and rauhwacke (Spengler, 1921; Cornelius, 1936; Kristan-Tollmann & Tollmann, 1967). To the NE, the thickness of the nappe is greatly reduced and while the cover sequence extends continuously to Gloggnitz, the basement rocks are phyllonitized and appear only discontinuously in a klippe at Mahdtalkogel and at Tratenkogel (Tollmann, 1977).

So far, no metamorphic peak conditions have been determined for the Troiseck Complex, but Late Devonian ages constrain cooling from amphibolite-facies metamorphic conditions (Handler, 1994; Schmidt, 1999). Ar–Ar muscovite ages indicate mid-Carboniferous cooling (Dallmeyer et al., 1998). Permian ages of 284 Ma (Handler, 1994) and 255 Ma (Schmidt, 1999) from Rb–Sr analyses on magmatic white mica presumably represent Eo-Alpine rejuvenation of Variscan ages (Schuster et al., 2001). The Veitsch- and Silbersberg nappes of the Veitsch-Silbersberg Nappe System (Neubauer et al., 1994; Schuster, 2016) are located in a hanging wall position on the northern side of the Troiseck-Floning Nappe. They were overthrust in the course of the Eo-Alpine orogeny, leading to a retrogressive overprint of lower greenschist-facies metamorphic conditions in the footwall (Handler, 1994; Dallmeyer et al., 1998; Schmidt, 1999). The thermal peak at the base of the overlying Veitsch Nappe is constrained by Raman spectroscopy on carbonaceous material (416 ± 23 °C; Rantitsch et al., 2020).

Towards the south the Troiseck-Floning Nappe is underlain by the Lower Austroalpine Unit, i.e. the Rosskogel Nappe, with a north-dipping tectonic contact that experienced ductile deformation under greenschist-facies metamorphic conditions in Late Cretaceous times (Dallmeyer et al., 1998; Schuster et al., 2001).

Miocene faults truncate this nappe pile, in particular the Mur-Mürz fault system in the East and the Trofaiach Fault in the Southwest (Fig. 2). The Trofaiach Fault is an east–west trending sinistral strike-slip fault (Nievoll, 1985) that constitutes the boundary between the Troiseck-Floning Nappe and the Seckau Nappe. The latter comprises the Seckau-, Amering-, and Speik Complexes (cf. Becker, 1980; Pfingstl et al., 2015; Mandl et al., 2018; 2022) which at least partly represent the lateral continuation of the Troiseck Complex.

2.2 Rosskogel Nappe

Permian silicic and intermediate metavolcanic rocks (also referred to as "Rosskogel Porphyroid" and "Biotite-Uralite-Schist", respectively) and Permian to Mesozoic metasediments are the main constituents of the Rosskogel Nappe (Cornelius, 1952; Gaal,

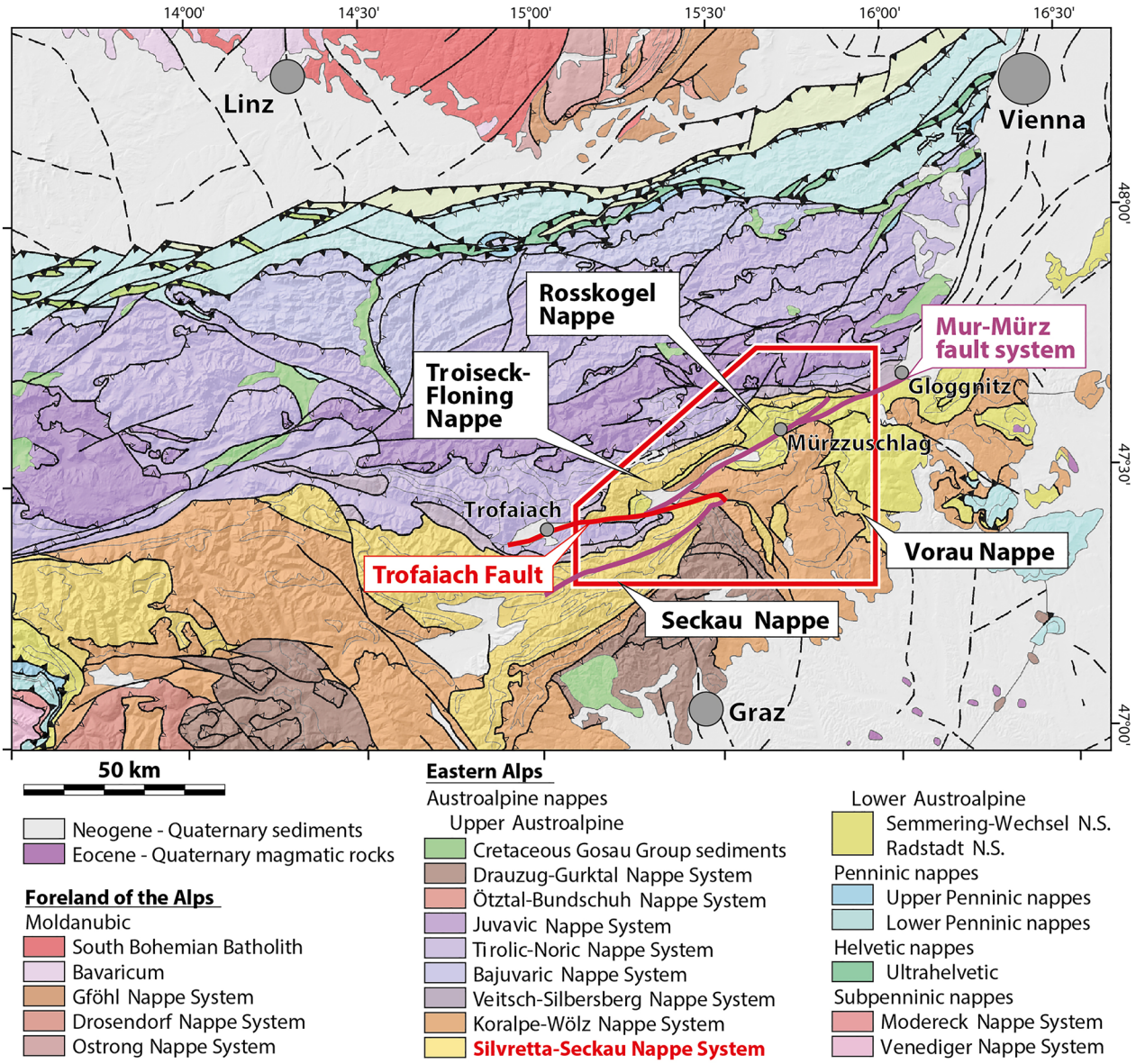

Fig. 2 Tectonic map of the northwestern part of the Eastern Alps based on a database of GeoSphere Austria in scale 1:500.000. The main tectonic features of the working area are indicated. The red polygon indicates the area visualized in Fig. 3

1965; Tollmann, 1977). The biotite-uralite-schists are exclusively occurring in the Rosskogel Nappe and in the (inverted) Lower Austroalpine Permian to Mesozoic rocks that appear in the footwall of the Troiseck Complex southwest of the proper Rosskogel Nappe. The rocks of the Rosskogel Nappe experienced strong internal ductile deformation and folding, which precludes the assignment of stratigraphic ages. Based on the metamorphic overprint of post-Variscan sequences, Gaal (1965) postulated a prograde Alpine overprint for the Rosskogel Nappe.

3 Analytical techniques

In the course of detailed mapping for the GK50 map sheets 102 Aflenz (Bryda et al., 2020) and 103 Kindberg, we took samples from main lithologies (metasedimentary and igneous rocks) of the Troiseck-Floning and Rosskogel nappes. Coordinates of sample locations are provided in Table 1. Thin sections (Fig. 3) were prepared and analyzed using an optical microscope. Sample preparation included crushing, sieving and standard mineral separation for zircon and biotite. We selected six samples from the Troiseck-Floning Nappe and two samples from

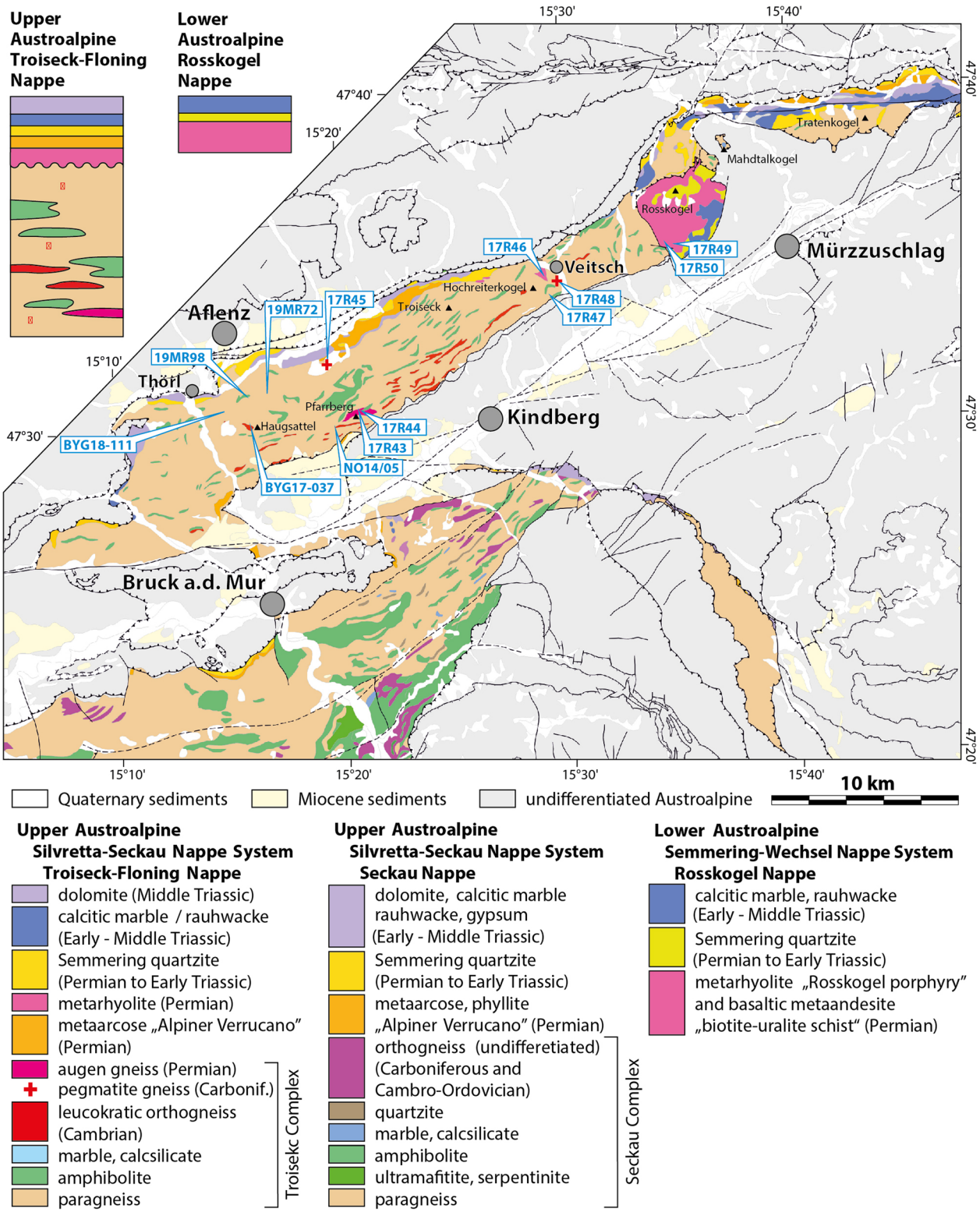

Fig. 3 Geological map showing the lithological content of the Troiseck-Floning, Seckau and Rosskogel nappes based on a database of GeoSphere Austria in scale 1:200.000. The principal rock columns of the Troiseck-Floning and Rosskogel nappes are visualized in the upper left corner. Sample localities are indicated on the map (coordinates are given in Table 1)

Table 1 Sample locations and analytical methods

Sample Name	UTM_northing	UTM_easting	Lithology	Lithostratigraphic unit/tectonic unit	Method		
					Whole-rock geochemistry	U–Pb zircon	Rb–Sr biotite
19MR98	5262483	519723	Garnet-amphibolite	Troiseck Complex/ Troiseck-Floning Nappe	x		
19MR72	5262686	521453	Amphibolite	Troiseck Complex/ Troiseck-Floning Nappe	x		
BYG17-037	5260844	520121	Haugsattel leucogranite gneiss	Troiseck Complex/ Troiseck-Floning Nappe	x	x	
BYG18-111	5262286	518831	Haugsattel leucogranite gneiss	Troiseck Complex/ Troiseck-Floning Nappe	x		
NO05/14	5260840	524846	Leucogranite	Troiseck Complex/ Troiseck-Floning Nappe			x
17R43	5261825	526175	Pfarrberg augen gneiss	Troiseck Complex/ Troiseck-Floning Nappe	x	x	
17R44	5261629	525882	Pfarrberg augen gneiss	Troiseck Complex/ Troiseck-Floning Nappe	x		
17R45	5264382	523838	Pegmatite gneiss	Troiseck Complex/ Troiseck-Floning Nappe	x	x	
17R46	5269066	536357	Metarhyodacite	Troiseck Complex/ Troiseck-Floning Nappe	x	x	
17R47	5268147	536640	Paragneiss	Troiseck Complex/ Troiseck-Floning Nappe	x	x	x
17R48	5268711	537324	Pegmatite gneiss	Troiseck Complex/ Troiseck-Floning Nappe	x	x	
17R49	5270374	543547	Metarhyolite	Rosskogel-Porphyry/ Rosskogel Nappe	x	x	
17R50	5270520	543324	Metaandesite	Rosskogel-Porphyry/ Rosskogel Nappe	x	x	x

metavolcanic rocks of the Rosskogel Nappe for U–Pb dating of zircon. Additionally, biotite from three samples was separated for Rb/Sr geochronology.

3.1 Whole-rock geochemistry

A representative aliquot of each sample, milled to a homogenous powder was shipped to Activation Laboratories Ltd facilities in Ontario/Canada where major and trace element analyses were carried out following the analytical procedure termed 'Code 4LITHO'. Major element composition and Sc, Be, V, Ba, Sr, Y and, Zr contents were analyzed using fusion inductively coupled plasma-optical emission spectroscopy (ICP-OES), while fusion ICP-mass spectrometry (ICP-MS) was used for all other trace-elements. Calibration was performed during the analysis using one of 14 prepared USGS and CANMET certified reference materials for every group of ten samples. Three blanks and five controls (three before the sample group and two after) were analyzed per group of samples. Duplicates were fused and analyzed every 15 samples, and the instrument was recalibrated after every 40 analyses.

3.2 Zircon U–Pb geochronology

Zircons for U–Pb age dating were separated using standard techniques. For LA-MC-ICP-MS analysis, handpicked zircons were embedded in epoxy resin, grinded and polished to half of their thickness. Combined backscattered electron (BSE) and cathodoluminescence (CL) images were taken from all zircons to document their internal structure.

U–Pb dates were obtained using a MC-ICP-MS Nu Plasma II from Nu Instruments coupled to a 193 nm excimer laser from ESI/New Wave Research. Measurement conditions are presented in Additional file 1: Table S1. Spot analyses were conducted with 25 µm spot size, 5 Hz repetition rate and a sample fluence of ~ 2.7–2.8 J/cm^2. The laser was warmed up before each measurement by shooting 25 s at the shutter, which was followed by 15 s of sample ablation. The ablation aerosol was transported by a He gas flow (0.73–0.75 l/min) and mixed with Ar make-up gas (0.75 l/min) in a mixing bulb before introduction into the torch. A mixed Faraday-multiple ion counting array was used for detecting the ions. Data reduction was performed with the IOLITE v. 3.71 software package using the X_U-Pb_Geochron4 DRS (Paton

et al., 2010, Paton et al., 2011). A common lead correction was not applied. The accuracy of secondary standards Plesovice and 91500 was better than 2%. The propagated 2SE of single $^{206}Pb/^{238}U$ dates of secondary standards and samples ranges from 0.5 to 2.5%. Only dates showing less than 2% discordance, calculated as $\left(1-\frac{FinalAge206/238}{FinalAge207/235}\right)*100$, were used for calculation of weighted mean ages. Weighted mean $^{206}Pb/^{238}U$ ages were calculated using the *IsoplotR* online software package (Vermeesch, 2018). The weighted mean age plots show uncertainties at 2σ level. Additionally, an external uncertainty was propagated and added quadratically to the uncertainty of the weighted mean ages. The approximate amount of the external uncertainty was estimated from the long-term excess variance of the secondary standards (~ 1.3%). The full dataset including analyses on reference zircons is provided in Additional file 2: Table S2.

3.3 Biotite Rb–Sr geochronology

Biotite was separated from sieve fraction 0.2–0.3 mm using a vibration table, grinding in alcohol and magnetic splitting. The weights of the samples used for dissolution were about 100 mg for whole-rock powder and ~200 mg for biotite. Chemical preparation was performed at the Geological Survey of Austria in Vienna. The chemical sample preparation follows the procedure described by Sölva et al. (2005). Isotope measurements were carried out at the Department of Lithospheric Research at the University of Vienna. Rb and Sr concentrations were determined by isotope dilution using mixed Rb–Sr spikes. Spiked Rb ratios were measured from Ta single filaments, whereas spiked Sr ratios were analyzed from Re double filaments with a ThermoFinnigan®Triton TI TIMS. Total procedural blanks are < 1 ng for Rb and Sr. During the periods of measurements the NBS987 standard yielded $^{87}Sr/^{86}Sr = 0.710248 \pm 4$ (n = 17; 2σ standard deviation). Isochron ages were calculated with the software IsoplotR (Vermeesch, 2018) assuming an error of 1% on the $^{87}Rb/^{86}Sr$ ratio.

4 Results

4.1 Petrography and geochemical characteristics

Thin section photographs are provided in Fig. 4. Results of major, trace and rare earth element (REE) analyses are provided in Additional File 3: Table S3. Plots of geochemical analyses (Figs. 5, 6 and 7) were generated with the software GeoChemical Data toolkit v6.0 (GCDkit; Janoušek et al., 2006).

4.1.1 Metabasites

Amphibolite bodies with transitions into hornblende-gneiss, intercalate with the metasediments of the Troiseck Complex. Generally, it is possible to distinguish two main types of amphibolite: banded plagioclase-rich amphibolite and characteristic garnet-amphibolite. Both types are mostly fine-grained with a layered structure subparallel to the main foliation. Locally, the rocks exhibit intense ductile deformation with rootless isoclinal folds and a pronounced hornblende mineral lineation. Thin (cm-thick) veins and patches of anatectic melt associated with coarse-grained hornblende presumably indicate initial stages of anataxis in structurally lower parts of the Troiseck Complex. Main minerals are amphibole, plagioclase, quartz, clinozoisite, epidote, biotite, chlorite, calcite and garnet. Apatite, zircon, ilmenite, titanite and rutile occur as accessory minerals. Hypidiomorphic to idiomorphic amphibole crystals are oriented in a nematoblastic fabric and show alteration to biotite and chlorite. The garnet-amphibolite shows characteristic kelyphitic rims, composed of fine-grained zoisite, quartz and plagioclase, around garnet porphyroblasts (Fig. 4a). Plagioclase exhibits alteration to sericite, clinozoisite and epidote. The latter also occur as zoned crystals in the matrix. Garnet and amphibole yield abundant inclusions of rutile (Fig. 4b), whereas in the matrix rutile occurs exclusively in the core of ilmenite and titanite. Thus, rutile presumably belongs to a first paragenesis overprinted by the main paragenesis comprising hornblende + plagioclase + quartz ± garnet + ilmenite ± titanite + apatite + zircon. The occurrence of actinolite + biotite + chlorite + hematite indicates a later retrograde overprint.

The metabasites show slight differences in composition that reflect their different appearance in the field. Both analyzed samples (sample 19MR72 from a banded amphibolite and sample 19MR98 from a garnet-amphibolite) classify as metabasalt with sample 19MR72 being richer in silica (51.5 wt % SiO_2) and Al_2O_3 (15.29 wt %), while sample 19MR98 yields a lower SiO_2 content (48.3 wt %), but higher Fe_2O_3 (15.6 wt %), TiO_2 (2.3 wt %) and MgO (7.2 wt %). Differences are also apparent in the calc-alkalic (19MR72) versus tholeiitic (19MR98) character (Hastie et al., 2007), the Zr/Y ratios (5.3 vs. 3), the LREE enrichment ($(La/Yb)_N = 4.34$ vs. 0.54) and an absent or only weakly negative Eu anomaly (Fig. 7a; $(Eu/Eu^*)_N = 1$ vs. 0.82). On the Zr–Nb–Y discrimination diagram (Meschede, 1986) sample 19MR72 plots in the field of within-plate tholeiite and island-arc basalt while sample 19MR98 classifies as N-MORB or island-arc basalt (Fig. 6a).

4.1.2 Metasedimentary rocks

Biotite-plagioclase-paragneiss and coarse-grained, garnet-bearing two-mica paragneiss together with mica schist represent the metasedimentary host rock. Quartz, biotite, muscovite, plagioclase (± alkali-feldspar) garnet ± hornblende are the main minerals. Locally, chloritoid overgrows the foliation in mica schists. The metablastic recrystallization of albite, the formation of titanite seams around ilmenite grains, as well as sericitization, chloritization, and saussuritization indicate a retrograde overprint. Plagioclase shows polysynthetic twinning and saussuritization. Biotite (showing rutile exsolution structures) and white mica are often intergrown, forming bent and kinked mica packages. Hypidiomorphic garnet up to several millimeters in diameter is often fully chloritized. Accessory minerals are apatite, zircon, tourmaline, zoisite, ilmenite, titanite and rutile. The latter is anhedral and abundant in the matrix, often mantled by ilmenite and as poikiloblastic inclusions in plagioclase. The chondrite-normalized Spider Plot (Fig. 7a) shows no Eu anomaly and exhibits a typical pattern for fine-grained sediments (McLennan, 2001). The enrichment of light Rare Earth Element (LREE) vs. heavy Rare Earth Element (HREE) presumably relates to the abundance of mica and heavy minerals.

4.1.3 Igneous rocks

Lenses of leucocratic granite gneiss, augen gneiss and pegmatite appear scattered across the metasedimentary host-rock of the Troiseck Complex. Still, the limited availability of outcrops hampers their correlation. The most important outcrops of plutonic rocks are located at the localities Haugsattel and Pfarrberg. Rhyolitic metavolcanics appear at the structural top, below the contact to the Mesozoic cover of the Troiseck Complex. All igneous rocks of the Troiseck-Floning Nappe fall into the granite (rhyolite for the metavolcanic rocks) field of the TAS classification diagram (Middlemost et al., 1994; Fig. 5a); the Zr/TiO_2 vs. SiO_2 diagram of Winchester & Floyd (1977) allows for the differentiation of the metavolcanic rocks (Fig. 5b). In the granite discrimination scheme of Frost & Frost (2008), the Haugsattel granite gneiss and the Pfarrberg augen gneiss show a ferroan trend, while the pegmatite samples plot in the magnesian field. The *Modified Alkali-Lime Index* (MALI; Frost & Frost, 2008; Fig. 5c), differentiates the granitoids of the Troiseck Complex into a calc-alkalic series (Haugsattel granite gneiss) and an alkali-calcic series (Pfarrberg augen gneiss); the pegmatite samples are partly alkali-calcic and calc-alkalic.

4.1.3.1 Haugsattel granite gneiss A leucocratic two-mica granite gneiss crops out at the Haugsattel on the main ridge of the Troiseck-Floning Nappe, with smaller lenses scattered across the Troiseck Complex. Quartz, alkali-feldspar, white mica, biotite and plagioclase (showing saussuritic and sericitic alteration) represent the main minerals. White mica often predominates over biotite. Hypidiomorphic garnet blasts and large, often zoned allanite crystals (up to 1 mm in diameter; Fig. 4c) locally intergrown with epidote/zoisite are characteristic. Biotite shows sagenitic rutile needles and partial replacement by secondary chlorite. The mica minerals are oriented parallel to a weak foliation. Other accessories are apatite and zircon.

The samples are characterized by a high silica (76.29 & 77.88 wt % SiO_2), intermediate Al_2O_3 content (11.65–12.28 wt %) and low Na_2O and CaO (3.07 & 3.83 wt % and 0.41 & 0.51 wt %, respectively) contents. The K_2O content is slightly elevated (5.01 & 3.56 wt %) with a K_2O/Na_2O ratio of 1.66 for sample BYG18-111. Both samples exhibit a ferroan character ($FeO_{tot}/(FeO_{tot}+MgO) > 0.8$; Frost & Frost, 2008) and plot in the calc-alkalic field (Fig. 5c). Low A/CNK values (molar proportions of $Al_2O_3/(CaO+Na_2O+K_2O) \leq 1.1$) for both samples indicate S-type to minor I-type affinity (Chappell & White, 2001). Trace and rare elements exhibit enrichment in Rb, U, K, Pb, Nd and show a strong depletion in Ba, Nb, Ta, Sr, P and Ti as well as relatively flat distribution patterns in HREE. On chondrite-normalized REE diagrams, these rocks show a pronounced negative Eu anomaly ($Eu/Eu^* = 0.11$ and 0.07; Fig. 7b). On the geotectonic discrimination diagrams, both samples plot in the field of volcanic-arc granites (VAG) and exhibit a similar source composition (Fig. 6b, c).

4.1.3.2 Pegmatite gneiss Small lenses of pegmatite gneiss occur frequently within the metasediments. The rocks are mainly composed of quartz, coarse-grained plagioclase (showing saussuritic and sericitic alteration) and white mica. Garnet, alkali-feldspar (microcline) and biotite appear subordinately. Allanite, apatite, zircon, titanite and epidote are present as accessory minerals. Epidote shows overgrowth of acicular zoisite. Both samples are silica-rich (73.8 & 74.03 wt % SiO_2) with high Al_2O_3 (16.68 & 15.01 wt %) and Na_2O (7.2 & 6.4 wt %) contents. K_2O is rather low (0.63 & 1.68 wt %) resulting in low K_2O/Na_2O ratios (0.09 vs 0.26). They are very poor in ferromagnesian elements ($Fe_2O_3^* + MgO + MnO + TiO_2 \leq 0.6$ wt %, $Fe_2O_3^*$ = total Fe expressed as Fe_2O_3). Several elements such as Nb, Ta, Yb, Y show low contents at or below the detection limit, while others, such as Ba (305

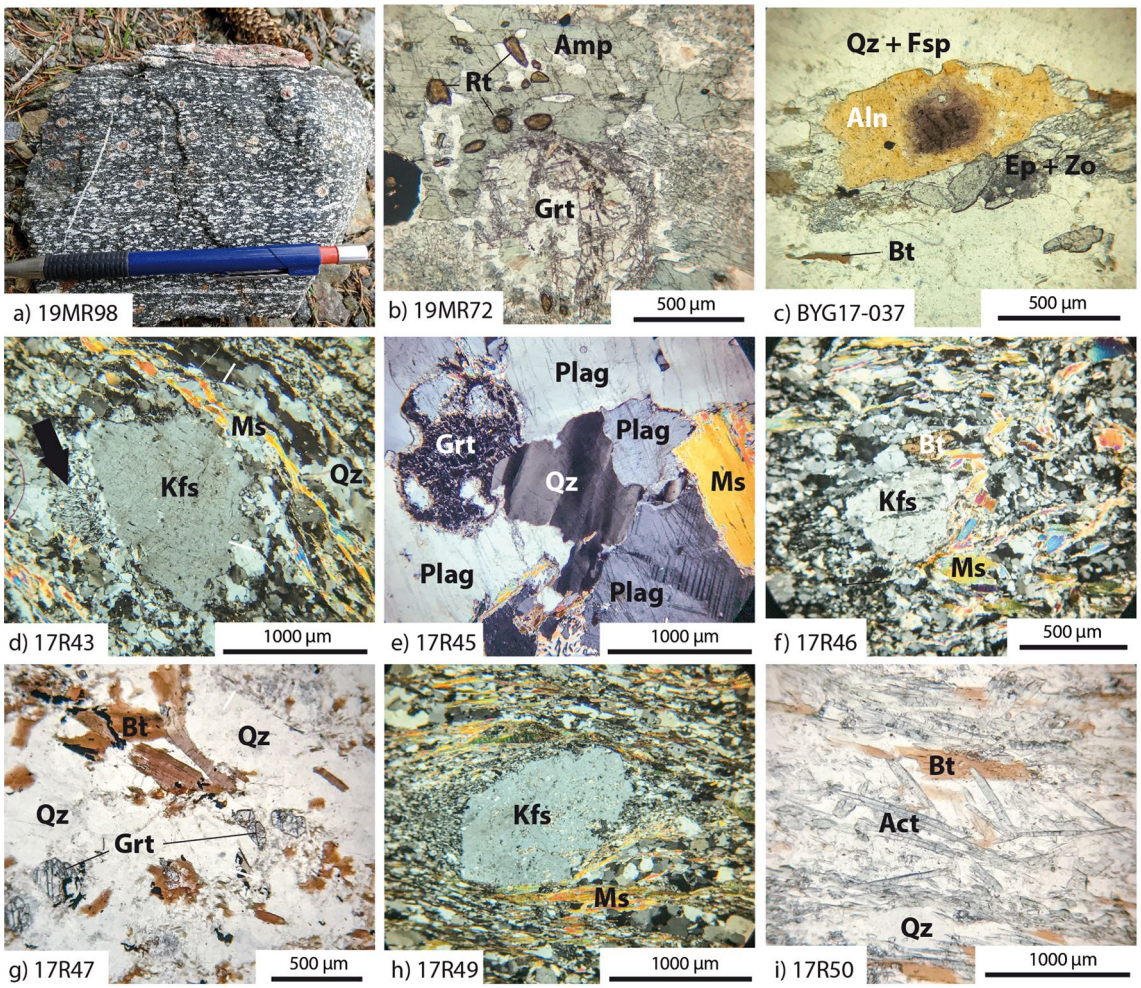

Fig. 4 Field and thin section photographs of representative samples. Abbreviations of mineral names according to Whitney & Evans (2010). **a** Garnet-amphibolite with characteristic kelyphitic rims around garnet (pen for scale). **b** Rutile inclusions in amphibole and in relictic garnet. **c** Large, zoned allanite minerals associated with zoisite and epidote in the Haugsattel granite gneiss. **d** Alkali-feldspar porphyroblasts in the fine-grained matrix; arrow points to small myrmekitic structures. **e** Amoeboid garnet surrounded by coarse-grained plagioclase, quartz and muscovite grains. Undulose extinction in quartz and flame-shape twinning in plagioclase (lower right corner) relates to deformation. **f** Aphanitic matrix with alkali-feldspar blasts in metarhyolite. **g** Large and unaltered biotite flakes in the paragneiss sample. **h** Porphyritic texture in metarhyolite showing a large, rotated alkali-feldspar blast in a fine-grained matrix composed of recrystallized quartz, plagioclase and muscovite. **i** Aggregates of acicular actinolite and large, unaltered biotite flakes in metaandesite of the Rosskogel Nappe

and 785 ppm for 17R45 and 17R48, respectively) and Sr (645 and 193 ppm) are abundant. Zr content is rather low ($\leq$30 ppm). In the chondrite-normalized REE diagram (Fig. 7c), sample 17R48 shows a flat profile with only very slight enrichment in LREE over HREE contents, while sample 17R45 shows no enrichment of LREE and depletion of HREE contents (analytical results mostly at or below the detection limit). Both samples exhibit positive Eu anomalies (Eu/Eu* = 2.45). Normalized to a primitive mantle (Fig. 7f), the samples are characterized by negative Ce, Pr, Nd and Ti anomalies and enrichments in Ba, Pb and Sr.

4.1.3.3 Pfarrberg augen gneiss In the southern part of the Troiseck-Floning Nappe, lenses of light-gray augen gneiss ("Helle Mikroklin-Augengneise"; Cornelius, 1936) intercalate with the metasediments e.g. at the locality Pfarrberg. The rocks form a few meters to a few tens of meters thick bodies and lenses subparallel to the main foliation that can be traced laterally over several kilometers. The rocks exhibit a mylonitic overprint with a pronounced subhorizontal stretching lineation. Alkali-feldspar porphyroblasts (2–8 mm in diameter) show inclusions of muscovite and quartz. The fine-grained matrix consists of

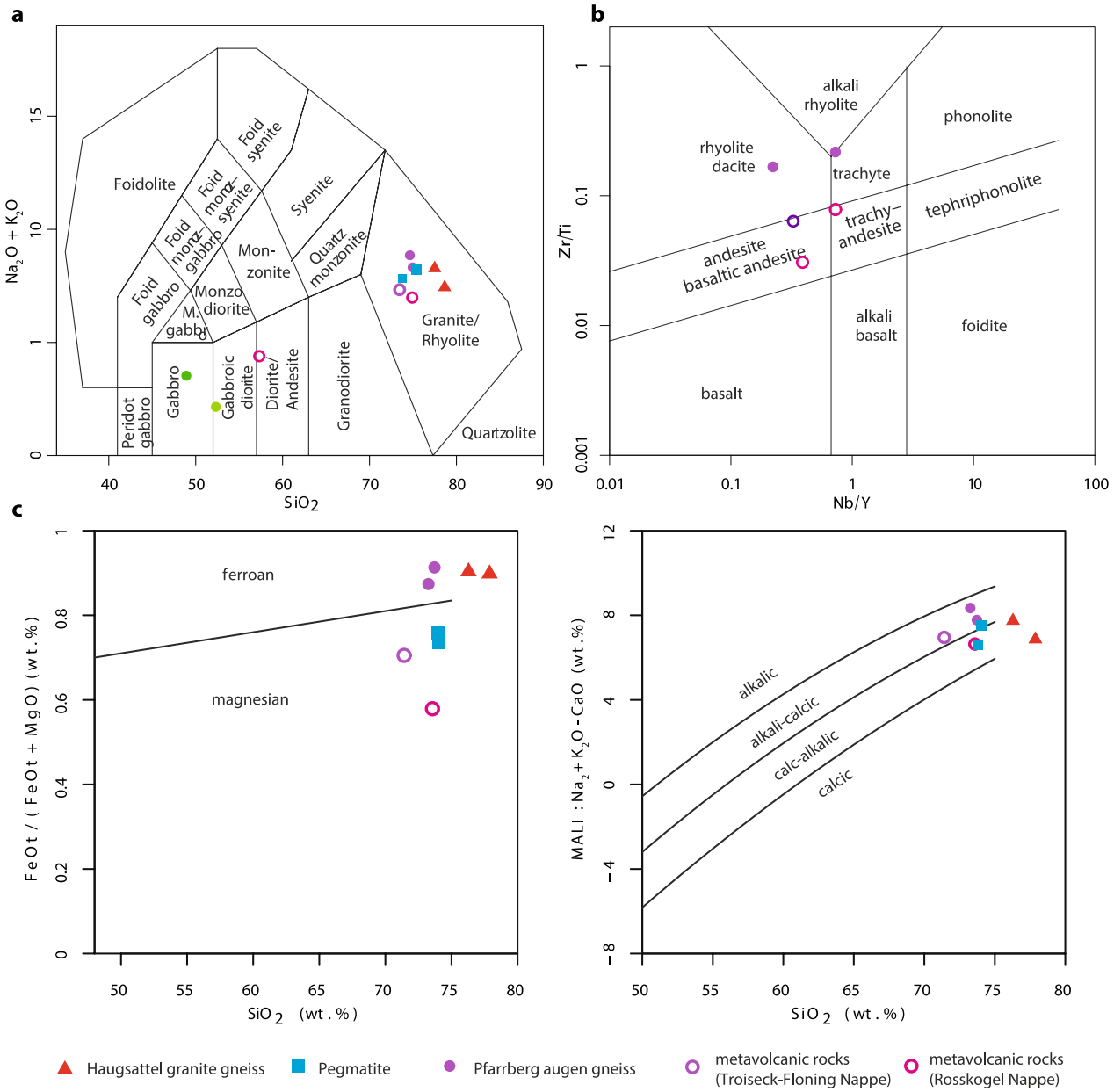

Fig. 5 Geochemical classification diagrams. **a** TAS (total alkali vs. silica; wt %) classification diagram (Middlemost, 1994). **b** Zr/Ti vs Nb/Y discrimination diagram for Permian volcanic rocks after Winchester & Floyd (1977) revised by Pearce (1996). **c** FeOt/FeOt + MgO vs SiO_2 (Fe index) and $Na_2O + K_2O$-CaO vs. SiO_2 (MALI: modified alkali lime index) of Frost et al. (2001)

quartz, feldspar, white mica/sericite and small, biotitized garnet blasts. Allanite, tourmaline, zoisite, rutile, ilmenite, epidote, apatite and zircon represent accessory minerals. The samples 17R43 and 17R44 exhibit high silica contents of 73.25 and 73.75 wt % while Al_2O_3 shows intermediate values (14.46–14.58 wt %). Na_2O (3.79 and 3.57 wt %) and K_2O content are slightly elevated (4.9 and 4.61 wt %) and the K_2O/ Na_2O ratio is 1.29 for both samples. According to the classification of Frost & Frost (2008), both samples show a ferroan character ($FeO_{tot}/(FeO_{tot} + MgO) > 0.8$) and are alkali-calcic, peraluminous (A/CNK ratio 1.19 and 1.26). The trace element geochemistry indicates enrichments in Cs, Rb, Ta, Pb, Sr and depletions in Ba, Nb, La, Ce, Pr, Sr, Eu and Ti. The Zr content is rather low for an orthogneiss ($\leq$40 ppm). On the chondrite-normalized REE diagram, both samples exhibit flat REE patterns ($(La/Yb)_N = 1.28–2.96$) and strongly negative Eu anomalies ($(Eu/Eu^*)_N = 0.06$ for sample 17R43; in sample 17R44 Eu

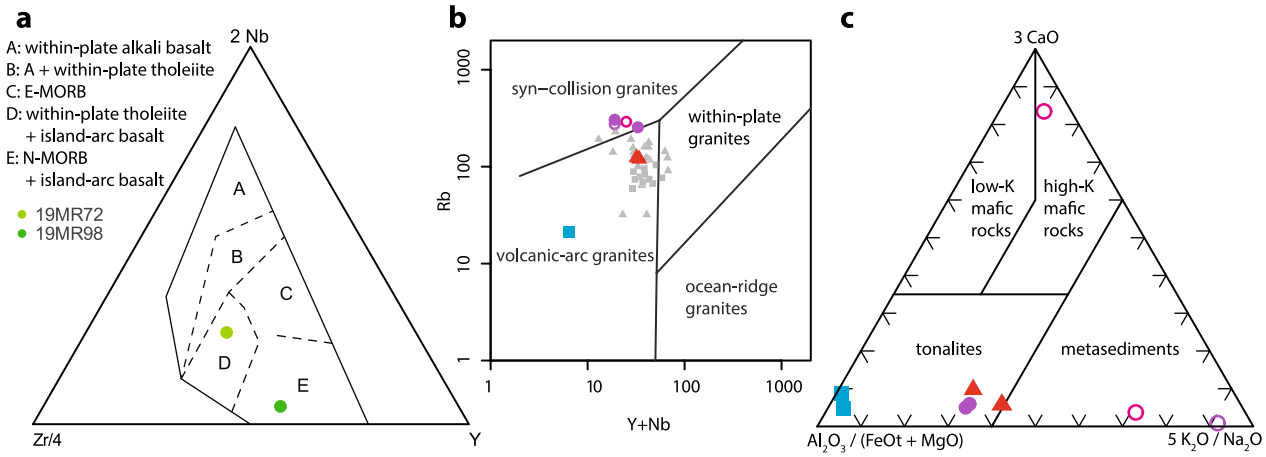

Fig. 6 Trace element tectonic discrimination plots. **a** Triangular plot of Zr/4-2Nb-Y after Meschede (1986). **b** Rb vs. (Y + Nb) plot (µg/g) after Pearce et al. (1984). Grey symbols represent data from Hintertal (square) and Hochreichart plutonic suites (triangle) presented in Mandl et al. (2022). **c** Source discrimination plot of Laurent et al. (2014). Symbols are the same as in Fig. 5

was below detection), which results in a seagull-shaped pattern (Fig. 7d; Glazner et al., 2008).

4.1.4 Metavolcanic rocks of the Troiseck-Floning and Rosskogel Nappe

The lowermost part of the Permian to Triassic cover of the Troiseck-Complex is dominated by volcaniclastic metasediments; metavolcanics termed "porphyroids" are subordinate. Porphyritic rocks are also exposed southwest of the village Veitsch at Hochreiterkogel where a slight synform of the Troiseck-Floning Nappe (fold axes in the southwest dip towards northeast and fold axes in the northeast dip towards southwest) causes the preservation of a relatively narrow, north–south elongated klippe on top of structurally higher parts of the basement. The metarhyolite of the Lower Austroalpine Rosskogel porphyry is very similar and locally preserved primary flow structures in less-deformed parts (Nievoll, 1986). Gaal (1965) classified them as Permian rhyolitic metavolcanics. Alkali-feldspar phenocrysts, rounded quartz pebbles (up to 3 cm in diameter), and pyroclastic particles (lapilli) are surrounded by a fine-grained matrix composed of quartz, sericite (parallel to the foliation) and albite. Deformed rocks exhibit a well-developed stretching lineation and show strongly altered magmatic feldspar crystals. In less deformed rocks, embayed quartz grains and glassy fragments in the matrix preserved their magmatic shape. Accessory minerals are zircon, allanite, rutile and ilmenite.

Dark-gray, biotite-rich metavolcanic rocks of andesitic composition (Gaal, 1965) are closely associated with the rhyolitic metavolcanic rocks of the Rosskogel Nappe. They are also referred to as "biotite-uralite schist" (Cornelius, 1952), which refers to the pseudomorphic growth of green actinolite after pyroxene (uralitization) occurring in these rocks. Thin sections show sericitized plagioclase, biotite, actinolite, chlorite, quartz, titanite and tourmaline. The porphyritic samples from both, the Troiseck-Floning Nappe (17R46) and the Rosskogel Nappe (17R49) are very similar in their major element composition and comparable to the Pfarrberg augen gneiss samples. The Zr/TiO_2 vs. SiO_2 diagram of Winchester & Floyd (1977; Fig. 5b) characterizes the samples as (meta)rhyodacite (sample 17R46), (meta)rhyolite (17R49) and (meta) andesite (17R50). A/CNK ratios of 1.76 and 1.58 indicate S-type granites. The chondrite-normalized REE diagram (Fig. 7d, e) shows LREE enrichment with a positive Ce anomaly and a negative Eu anomaly for sample 17R49 ($(Eu/Eu^*)_N = 0.19$). The metarhyodacite (sample 17R46) shows no fractionation ($(Eu/Eu^*)_N = 1.03$) and exhibits a similar trend as sample 17R50: a LREE enrichment with relatively flat chondrite-normalized MREE and HREE patterns (Fig. 7e).

The metaandesite sample (17R50; "biotite-uralite schist") shows a calc-alkalic signature with intermediate silica content of 55.81 wt % SiO_2. Al_2O_3 content is elevated (17.27 wt %), while Na_2O and K_2O contents are low (2.9 and 1.38 wt %, respectively), which results in a K_2O/Na_2O ratio of 0.48. High MgO and CaO contents of 5.44 and 6.44 wt % are characteristic.

4.2 Zircon U–Pb analyses

Cathodoluminescence (CL) images of zircon grains from representative samples of all magmatic rocks are

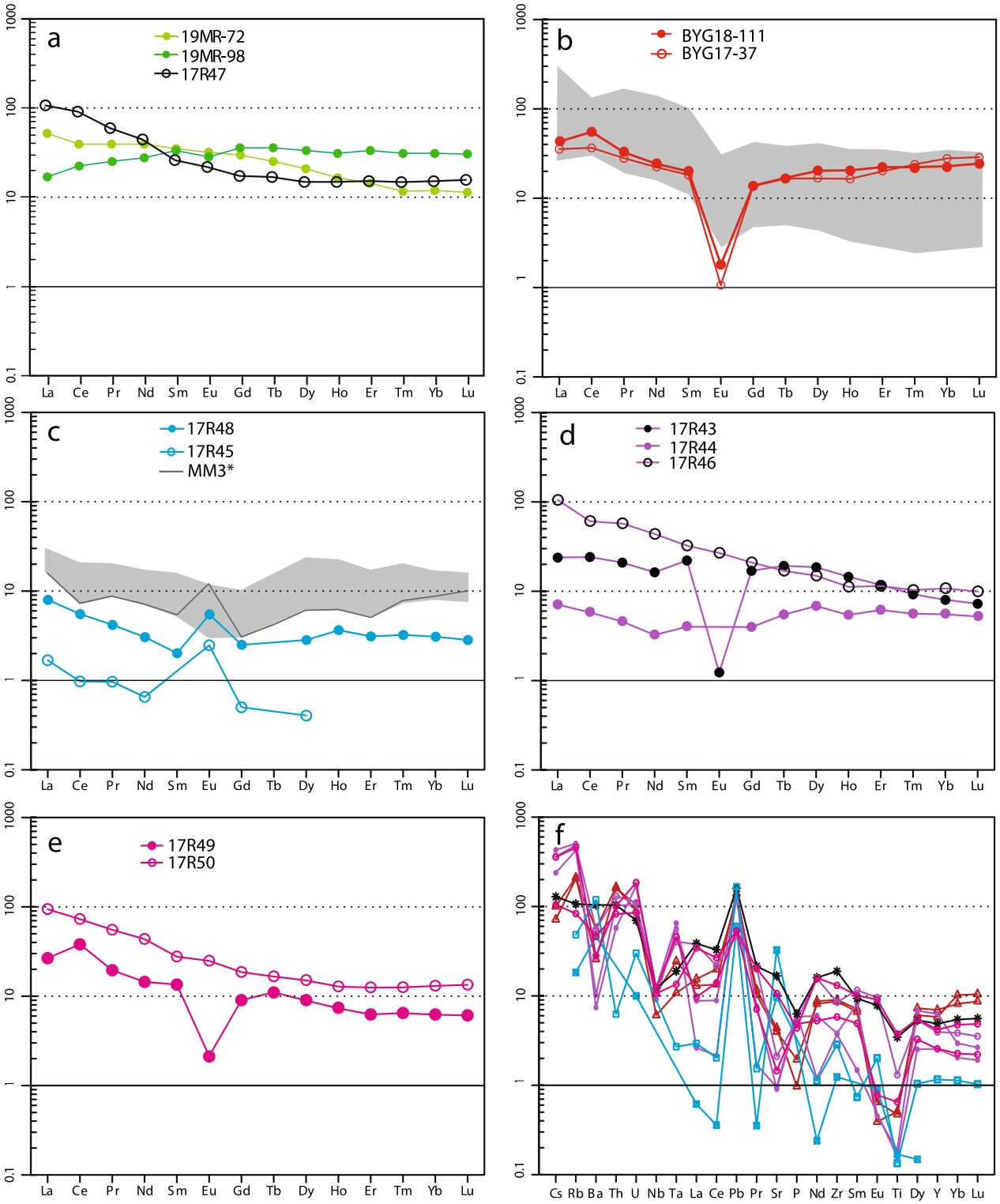

Fig. 7 Normalized multi-element diagrams ("Spider Plots"). Chondrite-normalized REE patterns and primitive mantle normalized trace element (µg/g) distribution patterns (normalization values after McDonough & Sun, 1995) of samples from the Troiseck-Floning Nappe and the Rosskogel Nappe. **a** Paragneis and metabasites. **b** Haugsattel granite gneiss. The gray field visualizes the data from the corresponding Hochreichart Plutonic Suite (Mandl et al., 2018; 2022). **c** Data from pegmatite gneiss lenses plotted together with data from pegmatitic dikes of the Seckau Nappe and sample MM3 (group 1; Mandl et al., 2018; 2022). **d** Permian plutonic and volcanic rocks from the Troiseck-Floning Nappe (Pfarrberg augen gneiss and metarhyodacite). **e** Metavolcanic rocks of the Rosskogel Nappe. **f** Primitive-mantle normalized REE plots

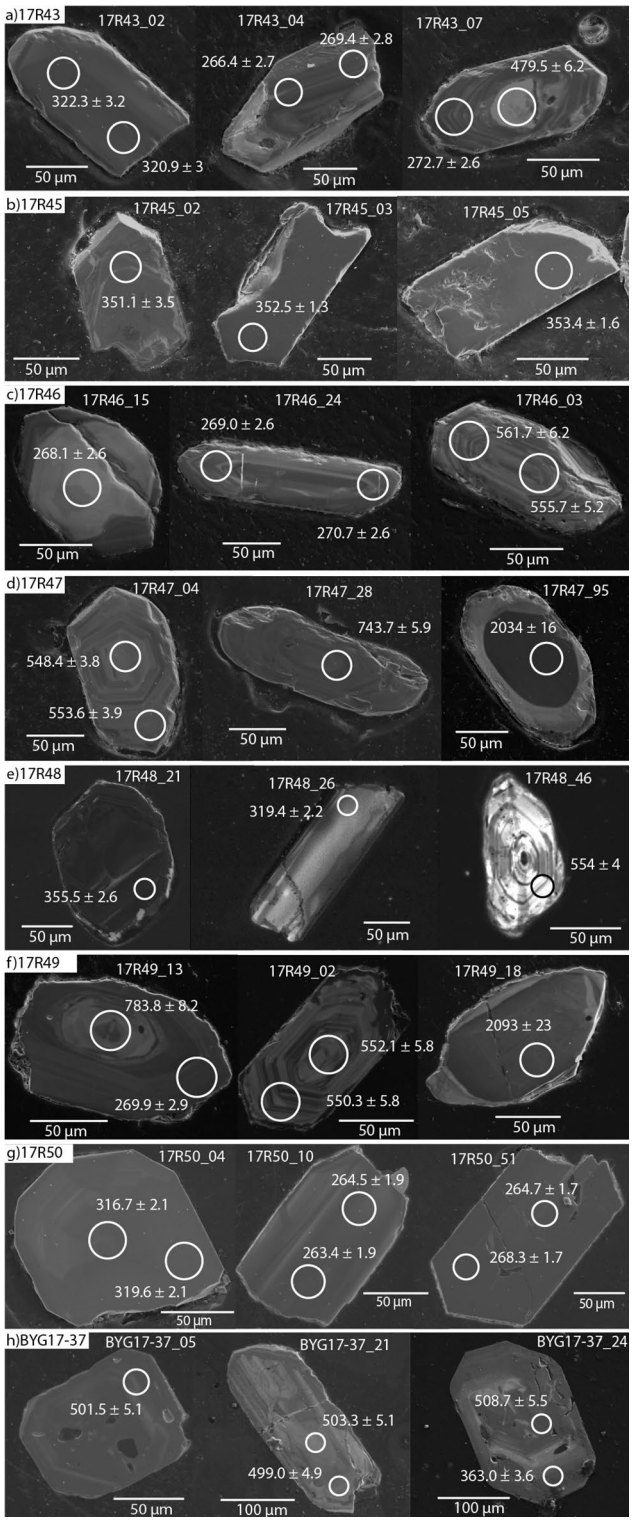

Fig. 8 Cathodoluminescence (CL) images of representative zircons: **a** Pfarrberg augen gneiss. **b** Pegmatite gneiss. **c** Metarhyodacite. **d** Paragneiss. **e** Pegmatite gneiss. **f** Metarhyolite. **g** Metaandesite. **h** Haugsattel granite gneiss. Targeted spots are indicated by a circle, spot date and propagated error are given

presented in Fig. 8. Most zircons show a well-developed growth-zoning pattern and display typical oscillatory zonation. U/Pb concordia diagrams and weighted mean ages are shown in Fig. 9. The dataset from detrital and inherited zircon grains is shown in Fig. 10.

4.2.1 Metasedimentary sample (detrital zircon analyses)

Detrital zircon grains of a garnet bearing paragneiss from the Hochreiterkogel near Veitsch (17R47) provide an Ediacarian weighted mean $^{206}Pb/^{238}U$ age of 553.0 ± 7.3 Ma (n = 56, MSWD = 1.7) for the youngest zircon population (Fig. 9d). The large zircon grains (~ 120–230 µm) are yellowish and show a rounded short prismatic to spindle shaped morphology (aspect ratios of 1:1.5–1:3). Smaller, rounded grains are often colorless. All grains show high Th/U ratios (> 0.5) that indicate a magmatic origin. Very few analyses yield lower Th/U ratios that do not represent a specific age population. Cathodoluminescence images show fine oscillatory zoning and xenocrystic cores, which yield Neoproterozoic (723.6–743.7 Ma, n = 3) and individual Mesoproterozoic, Palaeoproterozoic up to Mesoarchean ages between 1.0 and 2.9 Ga (Fig. 8d). To estimate the maximum depositional age (MDA) for the metasediments, we applied the 'Maximum Likelihood Age' (MLA) algorithm of Vermeesch (2021). The calculation resulted in a MDA of 541.8 ± 1.5 Ma.

Although the dataset of inherited grains in the metavolcanic sample from the Rosskogel Nappe (17R49) is just a byproduct and statistically not representative (n = 37), it nevertheless shows a similar late Ediacaran age peak (547.9 ± 7.3 Ma). A tentative comparison against the data from the Troiseck Complex (Fig. 10) shows a broader age range during the 450–580 Ma interval and several subpeaks at 631 Ma, 690 Ma, ~ 800 Ma and around 2 Ga for sample 17R49.

4.2.2 Haugsattel granite gneiss

Sample BYG17-037 yields euhedral, slightly rounded and mostly pink colored zircon crystals that are ca. 100–250 µm in length with a prismatic to pyramidal crystal habit (aspect ratios mostly 1:2; with up to 1:5 for long-prismatic grains). The sample yielded a mid-Cambrian weighted mean age of 502.4 ± 6.8 Ma (n = 12, MSWD = 1.7). A smaller subset of Early Ordovician ages (475.8 ± 6.4 Ma, n = 9) from grains with variable Th/U ratios (0.3—2.1) did not provide a statistically meaningful age (MSWD = 17). Wavy and irregular internal textures indicate recrystallization of the zircons from this subset. Latest Silurian (422.1 ± 6.4 Ma, n = 4) and scattered Devonian to Carboniferous ages (395.9–355.9 Ma) from overgrowth rims yield low Th/U ratios (< 0.1 or even < 0.01)

that indicate a (poly-)metamorphic overprint (Fig. 9h). However, the inclusion of Th-rich REE-minerals (allanite is present in thin sections) could also account for the low Th/U ratios in some crystals.

4.2.3 Pegmatite-gneiss

Crystals from both pegmatite gneiss samples are mostly euhedral spindle-shaped to prismatic (aspect ratios of 1:2—1:5) with red–orange-yellow tinted alteration colors. Zircon grains in sample 17R45 are characterized by high U (581.5–2369 ppm) and low Th contents (2.2—34.43 ppm), which results in very low Th/U-ratios 0.001–0.02 indicating either a metamorphic origin or relate to high fractionation in an anatectic environment. Sample 17R48 shows a higher variability (U: 117.7—4013 ppm; Th: 15.87–370.3 ppm) and a Th/U ratio ranging from 0.01 to 1.18. Together with resorbed internal shapes, this is indicative for dissolution-reprecipitation processes in both samples. To avoid these recrystallized parts, rims with oscillatory zoning were preferably targeted. The concordia plots (Fig. 9b, e) show several discordant data points, which presumably indicate Pb-loss during the overprinting of the cores.

The lower Mississippian weighted mean ages from both samples show a good agreement and overlap within error. Analysis of sample 17R45 provided a weighted mean age of 353.4 ± 4.9 Ma (n = 5, MSWD = 1.3), while sample 17R48 yields 353.4 ± 4.7 Ma (n = 7, MSWD = 1). A small subset of Pennsylvanian ages (~ 320 Ma, n = 4) can be observed in both samples, which is interpreted as (re-)crystallization age (Th/U ratio > 1.1). Sample 17R48 yields a few Cambrian to Cryogenian dates (~ 538.0 Ma, n = 2; 554 Ma; 699.5 Ma) from small, rounded and short-prismatic grains with Th/U ratios > 0.6 that presumably represent inherited grains either assimilated from the wall rock, or incorporated from the source.

4.2.4 Pfarrberg augen gneiss

The leucocratic augen gneiss from the Pfarrberg locality (sample 17R43) provides a mid-Permian weighted mean age (271.3 ± 3.6 Ma, n = 10, MSWD = 1.3; Fig. 9a). The paucity of zircon grains in this mylonitic gneiss calls for a meticulous mineral separation and sample preparation. Euhedral zircon crystals are ca. 70–200 µm in length with a prismatic crystal habit (aspect ratios mostly 1:1–1:2; with a few up to 1:4) and are usually transparent, occasionally weakly pink in color. A generally high Th/U ratio in combination with the absence of metamorphic overgrowth rims points towards a magmatic origin of the zircon grains. A subpopulation of subhedral grains that yield Pennsylvanian ages (weighted mean age: 322.1 ± 4.3 Ma, n = 5) are interpreted as inherited grains (Fig. 8a). The oldest ages were obtained from xenocrystic cores (479–636 Ma).

4.2.5 Metavolcanic rocks

The metarhyolite (metarhyodacite) sample from the Troiseck-Floning Nappe (17R46) provides a Permian (Guadalupian) weighted mean age of 268.6 ± 3.6 Ma (n = 12, MSWD = 1.8). The crystals are 100–200 µm in length, pink colored, spindle-shaped to long prismatic with aspect ratios of 1:2 – 1:4. Devonian, late Cambrian and Ediacarian ages (around 560 Ma) obtained from individual grains and xenocrystic cores represent inherited ages. The metarhyolite sample from the Rosskogel Nappe (17R49) yields a high number of inherited grains, which provide a wide spectrum of ages. The crystals are 100–200 µm in length, edge-rounded, spindle-shaped to prismatic (aspect ratios ~ 1:3) and often show a yellow tint due to alteration. Only two euhedral grains (Th/U ratio > 0.5) provided Permian (Guadalupian) ages of ca. 270.8 ± 2.6 Ma, which are interpreted as the crystallization age of the rock. Ordovician, Cambrian and Ediacarian dates (weighted mean ages: 459 ± 6.4 Ma, n = 3; 516.6 ± 7.4 Ma, n = 3; 547.9 ± 7.3 Ma, n = 16 and 621.6 ± 9 Ma, n = 3), as well as late Palaeoproterozoic dates obtained from individual grains (Fig. 8c) and xenocrystic cores represent inherited ages (Fig. 8f, 9f). The large number of inherited grains allows for a tentative comparison with the detrital zircon data from paragneiss sample 17R47 (Fig. 10).

Finally, zircon grains from a biotite-uralite schist (metaandesite; sample 17R50) are mostly broken fragments of euhedral crystals ca. 150–200 µm in length with a yellow tint due to alteration. The sample yields a Permian weighted mean age of 264.3 ± 3.5 Ma (n = 17, MSWD = 1.4). Interestingly enough, when the youngest ages from this dataset are excluded, we obtain a slightly older and statistically slightly less robust weighted mean age of 267.62 ± 3.5 Ma (n = 13, MSWD = 2.7) that possibly relates to antecrystic zircons or extended growth in a magma chamber before eruption. Th/U ratios of all analyzed grains are higher than 0.5, indicating a magmatic origin of the zircon crystals. Two analyses from an inherited grain provided Pennsylvanian ages (316.7 and 319.6 Ma).

4.3 Biotite Rb–Sr analyses

The results of Rb–Sr geochronology are summarized in Table 2, related Rb–Sr biotite ages are displayed in Fig. 11. The investigated biotite grains are unaltered (Fig. 4g, i). Two samples from the Troiseck-Floning Nappe were analyzed: biotite from paragneiss sample 17R47 and leucogranite sample NO14/05 yielded 75.4 ± 1.5 Ma and 77.6 ± 1.5 Ma respectively. Biotite from metaandesite

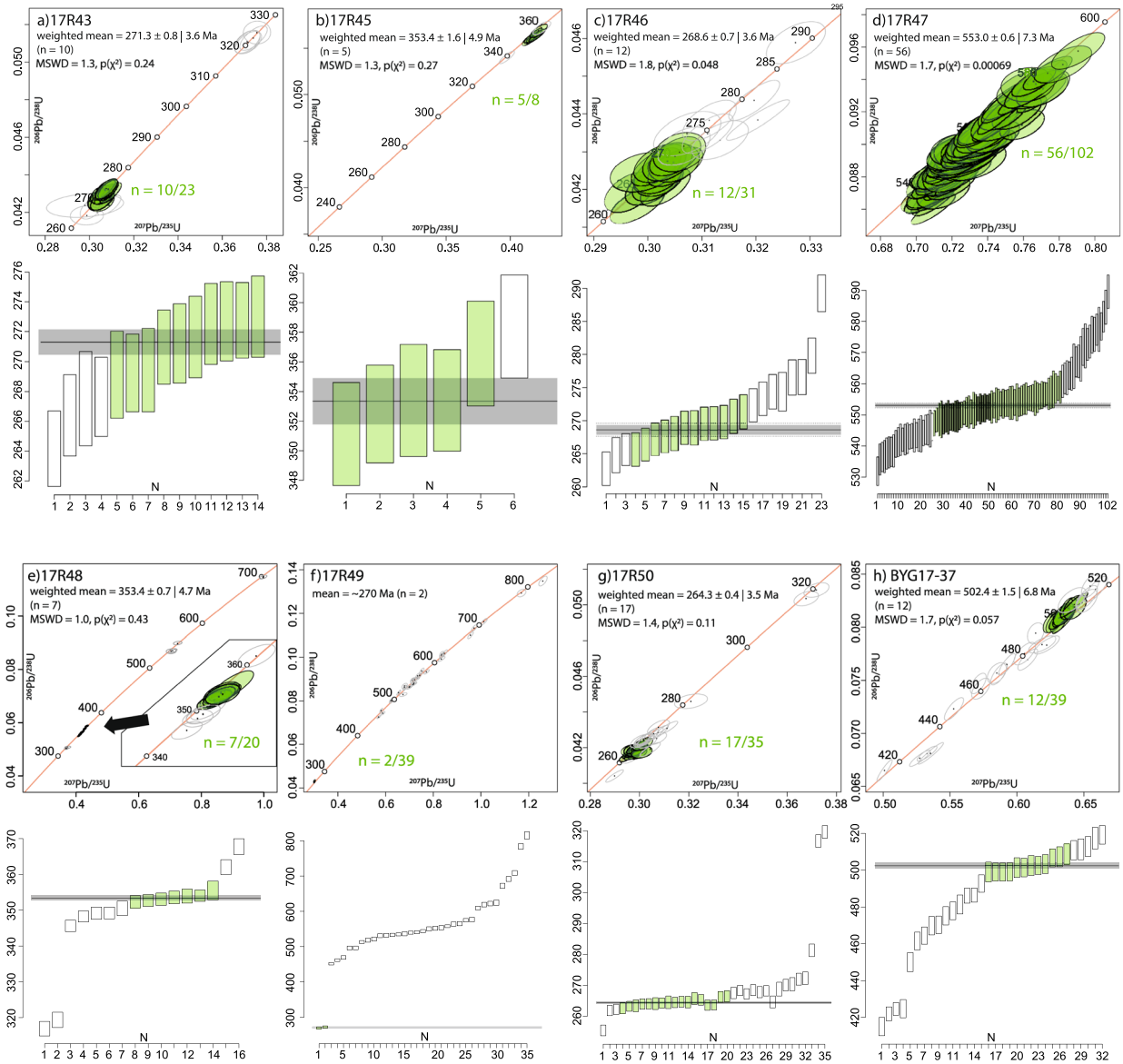

Fig. 9 U/Pb concordia and weighted mean diagrams: **a** Pfarrberg augen gneiss. **b** Pegmatite gneiss. **c** Metarhyodacite. **d** Paragneiss. **e** Pegmatite gneiss. **f** Metarhyolite. **g** Metaandesite. **h** Haugsattel granite gneiss. Weighted mean ages are provided with propagated errors and were calculated based on dates marked in green

(sample 17R50) of the Rosskogel Nappe provides an age of 76.7 ± 1.5 Ma. Taking their standard deviations into account, these ages are more or less identical within error.

5 Discussion

5.1 Geological evolution of the Troiseck-Floning Nappe from Neoproterozoic to Mesozoic times

Geochemical and geochronological data allow constraining the tectonometamorphic evolution of the Troiseck-Floning Nappe. This evolution is then compared against nearby crystalline basement complexes.

5.1.1 Paleogeographic constraints

Despite an ongoing discussion regarding the exact placement, there is a general agreement on the palaeogeographic position of the crystalline basement of the Silvretta-Seckau Nappe System at the northern margin of Gondwana during Neoproterozoic to Cambrian times (e.g. Mandl et al., 2018; Neubauer et al., 2020; Haas et al., 2020; Siegesmund et al., 2018; 2021). The dominance of a late Neoproterozoic detrital zircon population (attributed to the Cadomian and Pan-African orogenies), together with less frequent Meso- to Palaeoproterozoic and Archaean ages from xenocrystic zircon cores constrains

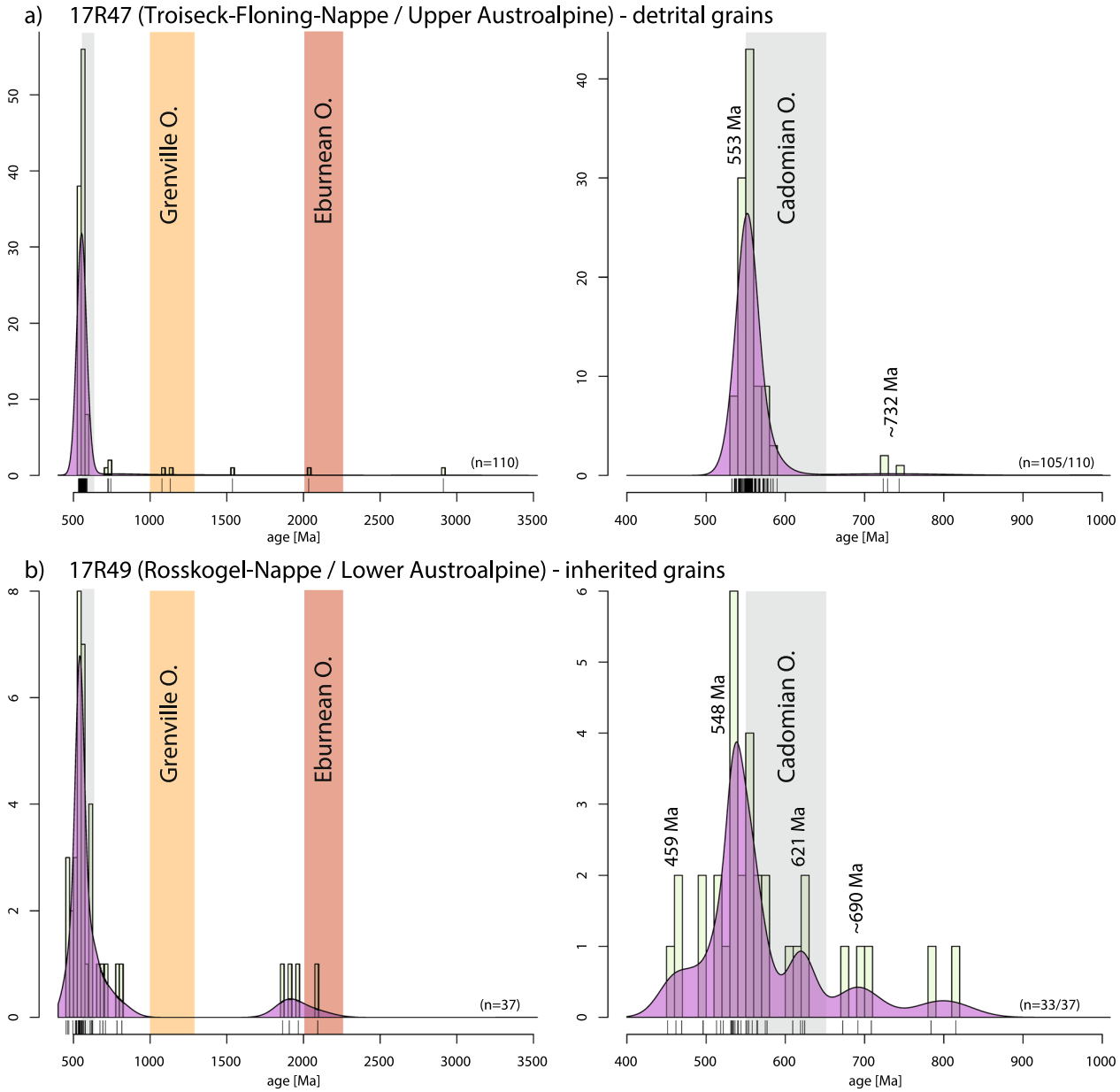

Fig. 10 Combined frequency and relative probability plots of detrital and inherited zircon grains. Diagrams show **a** detrital grains from the Troiseck-Floning Nappe and **b** inherited grains from the Rosskogel Nappe. Panels on the left show an age range from 400 to 3500 Ma (bin width = 25 Ma, bandwidth 35 Ma), panels on the right provide a more detailed view on the 400–1000 Ma age range (bin width = 10 Ma, bandwidth 15 Ma). Major orogenic events are given as colored boxes. Plotted using IsoplotR (Vermeesch, 2018)

influence from the Arabian-Nubian Shield/Sahara Metacraton (East African-Arabian Zircon Province; Stephan et al., 2019a; 2019b). Comparable detrital age distributions were obtained from the Glaneck metamorphic suite (Seckau Complex; Mandl et al., 2018), from the Tatric Unit of the Western Carpathians (Kohút et al., 2022) and from the Waldbach Complex (Vorau Nappe; Chang et al., 2021). However, the presence of a significant Ordovician peak (~ 450 Ma) in the latter is at variance with the previously mentioned datasets. Thus, in accordance with the palaeogeographic considerations of other authors (e.g. Haas et al., 2020; Neubauer et al., 2022; Finger & Riegler, 2023) we localize the depositional area of the Troiseck Complex along the northeastern Gondwana margin close to the Arabian-Nubian Shield/Sahara Metacraton during Late Neoproterozoic times. The relative paucity of

Archean to Mesoproterozoic ages in our detrital dataset could reflect a separation from the Gondwana mainland (possibly by an evolving back-arc basin; Neubauer et al., 2022). Nevertheless, the absence of data might be only statistical and calls for a careful interpretation.

5.1.2 Late Ediacaran to Cambrian volcaniclastic sedimentation

The abundance of xenocrystic cores in the zircons of the Troiseck Complex shows the influence of a continental hinterland. Together with characteristic contents of immobile trace elements (e.g. Th, Nb, Y, Sc, Co) and typical La/Sc and Ti/Zr ratios in the geochemical signature of the rocks, they allow for the interpretation as continental island arc sediments (Bhatia & Crook, 1986). As Sr decreases due to the weathering of feldspar with increasing maturity, the high Sr content, together with low Cr and Ni, which are adsorbed by clay minerals, indicate low maturity of the sediments. The detrital age record from the Troiseck Complex shows a dominant peak of Ediacaran to early Cambrian zircon ages that indicate a strong influence of Cadomian magmatism in the hinterland. The estimated maximum depositional age (541 ± 1.5 Ma) constrains the deposition of siliciclastic metasediments from late Ediacaran times onwards. The lack of geochronological data from the intercalated amphibolite layers restricts their interpretation. Nevertheless, the geochemical properties of banded amphibolite (calc-alkalic) and garnet-amphibolite (tholeiitic) from the Troiseck and Seckau complexes show a good agreement (cf. Neubauer, 1988). Tectonic and magmatic processes in a subduction-accretion complex (Zurbriggen, 2020), could account for the different trends in the geochemical composition of the amphibolite. Altogether, the metasediments of the Troiseck Complex show a good correlation with other late Ediacaran to Cambrian volcaniclastic metasedimentary sequences from the Silvretta-Seckau Nappe System (Mandl et al., 2018; Chang et al., 2021; Huang et al., 2021; Siegesmund et al., 2023). Despite the limited dataset, the age spectra of inherited zircon cores from metavolcanic rocks of the Rosskogel Nappe show significant differences to those of the Troiseck-Floning Nappe, with respect to the shape and distribution of the age peaks. However, the overlap in weighted mean ages from detrital zircon populations (553.0 ± 7.3 Ma sample 17R47 vs. 547.9 ± 7.3 Ma sample 17R49) indicate a common hinterland. Furthermore, the age distribution for sample 17R49 shows good agreement with results from the Wechsel Nappe (Lower Austroalpine Unit; Neubauer et al., 2020).

Moreover, since the presented detrital age record is not compatible with the detrital age distribution obtained from lower Triassic quartzite of the Permian to Mesozoic cover, both nappes disqualify as source areas and presumably were not exposed at the surface during the Early Triassic (Haas et al., 2020).

5.1.3 Cambrian/Ordovician emplacement of volcanic arc granites

The mid-Cambrian intrusion age (502.4 ± 6.8 Ma) of the Haugsattel granite gneiss shows a good agreement with other mid-Cambrian to Ordovician granitic intrusions from neighboring basement complexes of the Silvretta-Seckau Nappe System (i.e. Seckau Complex, Mandl et al., 2018; Waldbach Complex, Chang et al., 2021; Gollingand Riesach Complex, Huang et al., 2021). The ferroan calc-alkalic signature of the Haugsattel granite gneiss is indicative for partial melting of quartzo-feldspathic igneous sources (Frost & Frost, 2011; Frost et al., 2016) and the discrimination diagram of Pearce (1984) displays geochemical characteristics of volcanic-arc granites, which allows the correlation with the Hochreichart plutonic suite of Mandl et al., (2018; 2022). Accordingly, the Haugsattel melt intruded the volcaniclastic metasediments of the Troiseck Complex along an active peri-Gondwana margin during mid-Cambrian times. This allows for ambiguous interpretations either (i) as a late-stage intrusion along the Cadomian arc (Linnemann et al., 2014; Burda & Klötzli, 2011), (ii) as an early stage intrusion related to the Cenerian orogeny (490 – 440 Ma; Zurbriggen, 2017) or (iii) as intrusions related to the mid-Cambrian closure of Late Neoproterozoic to Cambrian back-arc basins (von Raumer & Stampfli,

Table 2 Rb–Sr isotopic data on biotite and whole-rock from the Troiseck-Floning and Rosskogel nappes

Sample	Material	Rb [ppm]	Sr [ppm]	87Rb/86Sr	87Sr/86Sr	2Sd(m)	Age [Ma]
17R50	WR	49.41	205.5	0.6961	0.710466	0.000004	
17R50	Bt	386.0	8.500	133.27	0.852589	0.000025	76.7 ± 1.5
17R47	WR	64.84	323.7	0.5799	0.711162	0.000004	
17R47	Bt	330.4	6.130	158.48	0.877528	0.000021	75.4 ± 1.5
NO14/05	WR	129.7	105.9	3.5484	0.727248	0.000005	
NO14/05	Bt	534.8	1.580	1094.5	1.909890	0.000020	77.6 ± 1.5

Analytical techniques are described in text. Ages were calculated from biotite (Bt) and corresponding whole-rock (WR) assuming an error of ± 1% on the $^{87}Rb/^{86}Sr$ ratio

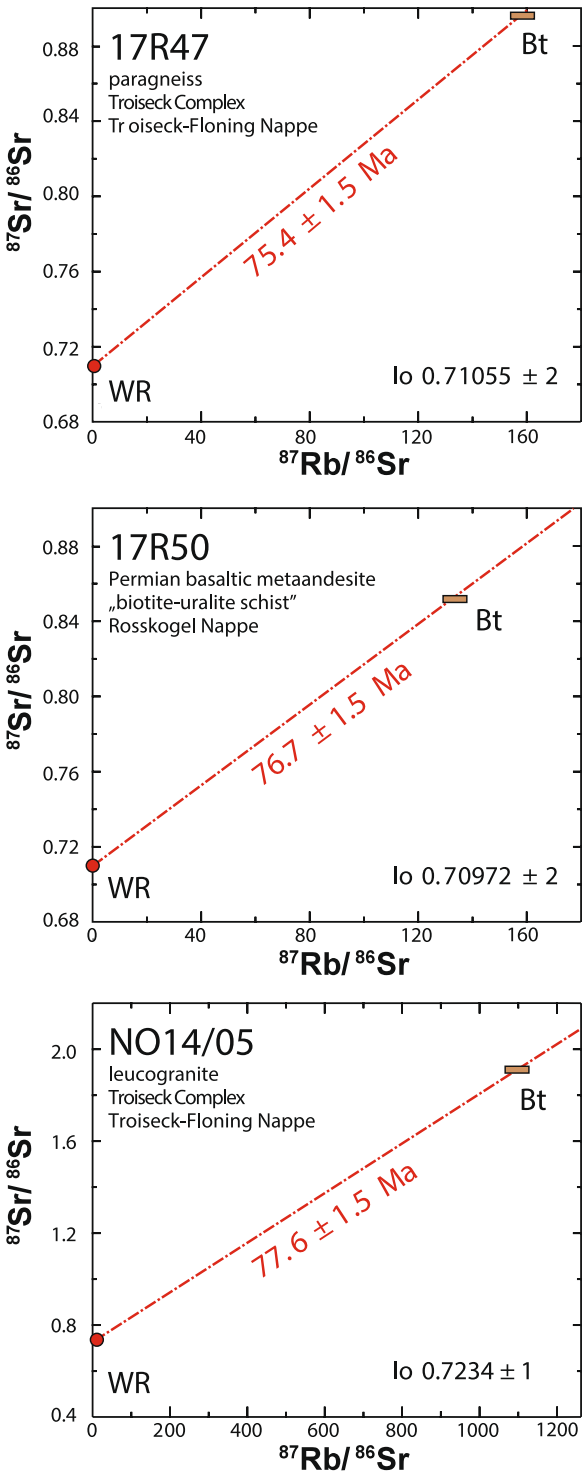

Fig. 11 Rb–Sr biotite–whole-rock ages from the Troiseck-Floning and Rosskogel nappes. Age calculation with IsoplotR and analytical results given in Table 2

2008). Of special interest in this context is the interpretation of ultramafic rocks from the Speik Complex (Seckau Nappe) as suboceanic mantle of an oceanic basin that underwent melting in a supra-subduction zone setting during the early Cambrian (Melcher & Meisel, 2004). (iv) A fourth scenario (following the model of Finger & Riegler, 2023), proposes margin-parallel transport of basement complexes (such as the Troiseck and Seckau complexes) and their subsequent incorporation in two separate Cadomian and Cenerian orogens (located in front of the Sahara Metacraton and the Arabian-Nubian Shield, respectively). Ordovician ages of recrystallized zircon grains with variable Th/U ratios from the Haugsattel granite gneiss indicate ongoing magmatism and accompanying metamorphism, probably during the Cenerian orogeny.

5.1.4 Devonian to Carboniferous metamorphism and granite emplacement

Parts of the Silvretta-Seckau Nappe System experienced high-pressure metamorphism during the Variscan orogeny (Faryad et al., 2002; Thöni, 2006). A subsequent and pervasive amphibolite-facies metamorphic overprint mostly obliterated the earlier overprint, but rutile inclusions observed in garnet and amphibole crystals (sample 19MR98) could represent remnants of a high-pressure paragenesis. Scattered Devonian to earliest Carboniferous ages from metamorphic overgrowth rims on zircon grains from the Haugsattel granite gneiss, the emplacement of pegmatite dikes during the Mississippian (353.4 ± 4.7 Ma) and Late Devonian/Carboniferous post-metamorphic cooling ages (Handler, 1994; Schmidt, 1999) prove an early Variscan overprint of the Troiseck Complex. Late Devonian to early Mississippian granitic/tonalitic intrusions, pegmatitic dikes, and migmatization of metasediments and amphibolites (generation of trondhjemitic melt) are reported from the neighboring Seckau Nappe (Neubauer et al., 2003; Mandl et al., 2018; 2022). Similar successions are reported from the Tatric and Veporic Unit of the Western Carpathians (e.g. Putiš et al., 2009a; Gawęda et al., 2016; Kohút & Larionov, 2021; Broska et al., 2022). The studied pegmatite samples could therefore originate from (i) residual melts related to large plutonic bodies (cf. igneous source rock as indicated in Fig. 6c and good agreement between sample 17R48 and dike group 2 of Mandl et al., 2022 in Fig. 7d), (ii) anatectic melts from metasediments (Knoll et al., 2023) or (iii) magmatic differentiation following the partial melting of amphibolite (Neubauer, 1988; Neubauer et al., 2003). The

peculiar chemical properties (plagioclase-rich, low-K_2O, magnesian, calc-alkalic to weakly alkali-calcic, weakly peraluminous, sodic) as well as the geochemical and petrographical properties agree with a trondhjemitic-tonalitic composition and match the definition of TTGs (tonalite–trondhjemite–granodiorite) sensu-stricto (O'Connor, 1965; Frost et al., 2001; Moyen & Martin, 2012; Bonin et al., 2020). Field observations of restitic hornblende closely associated with veins of anatectic melt in the amphibolite show that the observed negative Ti and Nb anomalies and the positive Eu anomaly possibly correlates with the retention of hornblende at the site of partial melting (cf. Drummond & Defant, 1990). The strong LREE/HREE fractionation in sample 17R45 probably relates to melting of a garnet-bearing amphibolite (Rapp et al., 1991; Foley et al., 2002). On the other hand, these properties can also be explained by strong wall rock–pegmatite interaction, hydrothermal alteration and anatectic melting of metasediments.

Metamorphic overgrowth rims and inherited grains in several samples (320.3 ± 4.2 Ma, n = 12; samples 17R43, 17R45, 17R48, 17R50; Figs. 8, 9) yield evidence for late Variscan metamorphism (see also data from the Waldbach Complex; Chang et al., 2021). Pennsylvanian ages from Ar–Ar white mica analyses constrain post-metamorphic cooling and exhumation (Handler, 1994; Schmidt, 1999).

5.1.5 Permian magmatism in the Troiseck-Floning and Rosskogel nappes

Continental rifting and associated lithospheric thinning during Permian times led to decompression melting in the mantle lithosphere (Schuster & Stüwe, 2008). Accompanying mafic underplating and secondary crustal melting reportedly caused granite and pegmatite intrusions at mid-crustal levels and widespread high-temperature/low-pressure metamorphism in the Adria-derived units of the European Alps (e.g. Thöni and Miller, 2000; Thöni & Miller, 2009; Schuster et al., 2001). Permian intrusions, often associated with A-type affinity, are widely reported from the eastern periphery of the Alps (Knoll et al., 2018; Chen et al., 2020; Yuan et al., 2020; Huang et al., 2021; 2022) and from the Western Carpathians (Villaseñor et al., 2021; Ondrejka et al., 2021, and references therein). The presented Guadalupian intrusion age for the Pfarrberg augen gneiss (271.3 ± 3.6 Ma) shows a good correlation with the aforementioned studies. Although the Pfarrberg augen gneiss does not meet the classical criteria for A-type granites (Whalen et al., 1987), its ferroan, alkali-calcic and strongly peraluminous character is characteristic for high-temperature melting of crustal lithologies in a post-orogenic setting (Frost et al., 2001) and related to the assimilation of a greater amount of felsic crust (Frost & Frost, 2011). The geochemical signature evident in REE-plots (strong Eu-anomaly, flat REE profile; Fig. 7d) indicates extensive fractionation of plagioclase in a hot, dry magma (Bachmann & Bergantz, 2008).

Additional constraints on the timing of Permian magmatism come from metavolcanic rocks that cover the Troiseck-Floning Nappe and Rosskogel Nappe. Guadalupian ages from the porphyritic samples show a close chronological correlation, with the metarhyolite from the Rosskogel Nappe (271 Ma vs. 269 Ma). Thus, the effusive activity is coeval with the intrusion of the Pfarrberg augen gneiss. The presence/absence of a negative Eu-anomaly, together with Sr, Nd and Ti depletions observed in the metarhyolite samples are consistent with a magma that underwent a variable degree of fractional crystallization and moderate crustal assimilation. The quasi-contemporaneous calc–alkalic metaandesite of the Rosskogel Nappe (crystallization age of 264 Ma) indicates bimodal magmatism (cf. different source rocks in Fig. 6c), which is typically associated with rift-settings. This variability in the magmatic source of post-collision granites hampers their classification (Pearce, 1996). Therefore, although the Permian volcanic and plutonic rocks are associated with a post-collision setting, they plot in the field of syn-collision granites in the geotectonic discrimination diagram of Pearce et al., (1984; Fig. 5b). The high number of xenocrysts supports an extremely low zircon fertility of the Rosskogel porphyroid magma. Coeval calc-alkalic to subalkalic volcanic suites composed of andesite, rhyolite and rhyodacite (267 to 262 Ma) unconformably cover the metamorphic basement of the Infratatric and Veporic units in the Western Carpathians (Putiš et al., 2016; Vozárová et al., 2020). Andesitic volcanism, albeit of early Permian age, is reported from the Subpenninic Unit of the Tauern Window (Veselá et al., 2008), Briançonnais Unit of the Western Alps (Ballèvre et al., 2020) and the Southalpine Unit (e.g. Visonà et al., 2007).

5.1.6 Alpine overprint and post-tectonic exhumation

We associate ductile deformation and folding of the Permian to Lower Triassic metaconglomerate with deformation during the Eo-Alpine overprint (Reiser, 2020). Dallmeyer et al. (1996) reported a Late Cretaceous age (93.1 Ma; $^{40}Ar/^{39}Ar$ white mica) from Permian to Mesozoic cover sediments of the Troiseck-Floning Nappe. Together with pre-Alpine $^{40}Ar/^{39}Ar$ ages from the crystalline basement, the Eo-Alpine overprint is constrained to greenschist-facies metamorphic conditions (< 450 °C; Dallmeyer et al., 1998; Schmidt 1999). Ductile shearing of the tectonic contact between the Troiseck-Floning Nappe and the Rosskogel Nappe (e.g. mylonitic overprint in Fig. 4h) is constrained to about 81 Ma (Dallmeyer

et al., 1996; 1998). West of Mürzzuschlag, the latter rests inversely, i.e. tectonically, on phyllonitic metasedimentary rocks of the so-called Mürz-Tachenberg Nappe.

The presented $^{87}Rb/^{86}Sr$ analyses on biotite (75.4 ± 1.5 Ma and 77.6 ± 1.5 Ma from the Troiseck-Floning Nappe and 76.7 ± 1.5 Ma from the Rosskogel Nappe) show a good agreement with previously published $^{87}Rb/^{86}Sr$ analyses from the Troiseck-Floning and Seckau nappes (Handler, 1994; Dallmeyer et al., 1998; Schmidt, 1999; Pfingstl et al., 2015). Together, the data constrain Late Cretaceous cooling from greenschist-facies metamorphic conditions and exhibit a trend towards younger ages in the east (85 Ma vs. 75 Ma). Separation of the Troiseck-Floning and Seckau nappes along the Trofaiach Fault and a general strike-slip dominated fault regime occurred in the course of final cooling and exhumation of the study area during Oligocene/Miocene times (van Gelder et al., 2020).

5.2 Correlation of the Troiseck complex with neighboring units of the Silvretta-Seckau Nappe system

Retrodeformation of the sinistral displacement along the Trofaiach Fault juxtaposes the Troiseck-Floning Nappe against the Seckau Nappe. The latter comprises the Seckau, Amering, and Speik complexes (Becker, 1980 and compiled map of Pfingstl et al., 2015). Steeply inclined ductile shear zones, presumably of Alpine age, later partially reactivated as sinistral strike-slip faults, dissect the Seckau Nappe (Neubauer, 1988). The Speik Complex representing a pre-alpine ophiolite composed of amphibolite, ultramafic rocks and minor metasediments was emplaced on the Amering Complex along a Variscan(?) tectonic contact. The stronger Eo-Alpine overprint of the Amering Complex (Late Cretaceous cooling from amphibolite-facies metamorphic conditions; Neubauer et al., 1995) and the different geologic context of the Speik Complex preclude their correlation with the Troiseck Complex. While granitic intrusions occupy large areas in western parts of the Seckau Complex (Mandl et al., 2018), this predominance decreases towards the east where metasediments and metabasites were intruded by the Rennfeld tonalite (353 Ma; Neubauer et al., 2003). Although the Troiseck Complex predominantly consists of metasediments and metabasites with only scattered lenses of igneous rocks, the similar lithostratigraphy and geologic evolution, the laterally continuous fold structures, and the mutual low-grade Alpine overprint (less than 450 °C; Scharbert, 1981; Mandl et al., 2018; Pfingstl et al., 2015) show a good correlation between the Seckau and Troiseck complexes.

The Waldbach Complex of the Vorau Nappe, located to the southeast of the Troiseck-Floning Nappe, occupies a similar tectonic position in the hanging wall of the Lower Austroalpine Wechsel Nappe and below an element of the Koralpe-Wölz Nappe System (Stuhleck-Kirchberg Nappe). The tectonic contact between the Vorau and Wechsel nappes exhibits Late Cretaceous deformation under greenschist-facies metamorphic conditions (Dallmeyer et al., 1996; Schuster & Nowotny, 2016). The crystalline basement comprises two different lithological entities, the upper level is composed of granitic orthogneiss, hornblende gneiss, and amphibolite/metagabbro, while the lower level consists of quartzite, sulfidic blackschist and a thick layer of coarse-grained garnet-mica schist that are interpreted as Devonian metasediments (Flügel & Neubauer, 1984; Neubauer et al., 2022). The metasediments from the upper level of the Waldbach Complex represent a late Ediacaran to Cambrian juvenile magmatic arc that was intruded by Cambrian to Ordovician granitic bodies and which underwent (upper) amphibolite-facies metamorphism during the Variscan orogeny (Chang et al., 2021). Despite lithological differences in the lower part of the Waldbach Complex and a stronger retrogressive overprint during the Eo-Alpine evolution, both complexes occupy a comparable structural position and share a similar Cambro-Ordovician and Variscan evolution. Thus, we would like to point out the similarities between the upper part of the Waldbach Complex and the Troiseck Complex, especially in comparison to the other units below (Wechsel Nappe) and above (Stuhleck-Kirchberg Nappe).

5.3 Unravelling parallels between the Troiseck-Floning Nappe and the Western Carpathians

In this chapter, we would like to emphasize the similarities in the geological evolution of the Troiseck Complex and the Tatric and Veporic units of the Western Carpathians. Mandl et al. (2018) also pointed out parallels between the latter and the Seckau Complex. The crystalline basement of the Tatric Unit occupied a palaeogeographic position in the eastern domain of the Gondwana margin (Kohút et al., 2022), which is comparable to the position of the Seckau and Troiseck complexes (Mandl et al., 2018; this study). Both Tatric and Veporic units comprise medium to high-grade metamorphic rocks (e.g. Moussallam et al., 2012; Petrik et al., 2020; Burda et al., 2021; Janák et al., 2022), Cambro-Ordovician (Putiš et al., 2009a) and Late Devonian—early Carboniferous granitic intrusions (Gawęda et al., 2016; Uher et al., 2019; Kohút & Larionov, 2021; Broska et al., 2022; Catlos et al., 2022). Permian magmatism is widespread in the Western

Carpathians (e.g. Ondrejka et al., 2021; Villaseñor et al., 2021).

Lithostratigraphic units that constitute the crystalline basement of the Western Carpathians (cf. Putiš et al., 2009a) allow for potential correlations with previously described pre-Alpine basement complexes of the Seckau Nappe, Troiseck-Floning Nappe and Vorau Nappe. In the Tatric Unit, these subunits are referred to as upper and lower étage (Kohút et al., 2022). The lower étage comprises late Ediacaran to early Silurian migmatitic metasediments that intercalate with metabasites (amphibolite and remnants of retrogressed eclogite; Burda et al., 2021) and which were intruded by Cambrian–Ordovician and Late Devonian–early Carboniferous granitoids. Partly, the rocks experienced a Variscan eclogite-facies metamorphic overprint, followed by isothermal decompression and associated migmatization with trondhjemitic melt formation (Moussallam et al., 2012). This evolution shows great similarity with the pre-Alpine evolution of the Troiseck and Seckau complexes and with the upper level of the Waldbach Complex (Troiseck-Floning Nappe, Seckau Nappe and Vorau Nappe, respectively). The upper étage consists of late Silurian—Devonian volcaniclastic metasediments, metabasites (epidote-actinolite amphibolite), black shale and lenses of calc-silicate gneiss (Kohút et al., 2022), which might correspond to the lower level of the Waldbach Complex for which Neubauer et al. (2022) postulate a Devonian sedimentation age.

In the course of Cretaceous nappe stacking, the Tatric and Veporic units ended up in different structural positions. On a geological map of the Western Carpathians (Plašienka, 2018), the Tatric Unit occupies a structurally lower position in the NW. It only recorded a low-grade metamorphic Alpine overprint and the basement largely preserved its Variscan mineral assemblage and structure. In contrast, the Veporic Unit experienced Alpine ductile deformation and greenschist to lower amphibolite-facies metamorphism (Janák et al., 2001; Jeřábek et al., 2012; Plašienka, 2018; and references therein) with a thermal peak at ca. 100 Ma (Vojtko et al., 2016). Both, Tatric and Veporic units show syn-collisional exhumation from around 80 Ma onwards with a slightly earlier onset of exhumation for the latter (Putiš et al., 2009b; Králiková et al., 2014; 2016; Vojtko et al., 2016). With respect to the grade of Eo-Alpine overprint, the Troiseck and Seckau complexes are thus in the range of the Tatric Unit and northern parts of the Veporic Unit. Also, the timing of Late Cretaceous exhumation (Pfingstl et al., 2015; this study) and final cooling in the Cenozoic is similar (Kralikova et al., 2016; van Gelder et al., 2020). However, the internal style of the nappe stack in the Eastern Alps and Western Carpathians shows remarkable differences (Froitzheim et al., 2008), which precludes a one-to-one correlation of the units.

6 Conclusions

The combination of whole-rock geochemistry, U–Pb zircon dating and Rb–Sr biotite geochronology provides important constraints on the geological evolution of the Troiseck-Floning Nappe from Neoproterozoic to Mesozoic times. The Troiseck Complex developed from clastic sediments and basic volcanic rocks deposited at a juvenile continental magmatic arc along the northeastern Gondwana margin during late Ediacaran to mid-Cambrian times. In the late Cambrian to Early Ordovician (510–480 Ma), volcanic-arc granitoids intruded the volcano-sedimentary host-rock of the Troiseck Complex. Accompanying metamorphism correlates with the emplacement in an active margin setting.

In the course of the Variscan orogeny, the Troiseck Complex experienced deformation at amphibolite-facies metamorphic conditions and Late Devonian/early Carboniferous intrusions (~ 353 Ma) of calc-alkalic leucogranite bodies and pegmatite dikes. The latter indicate melting of a metasedimentary and/or amphibolitic protolith and presumably formed during exhumation after an early Variscan metamorphic overprint. A second overprint during Carboniferous times (~ 320 Ma) relates to a late Variscan event.

The deposition of Permian clastic sediments and rhyolitic to andesitic volcanic rocks (271–264 Ma) constrains a surface position of the Troiseck Complex and the former basement of the Rosskogel Nappe during Permian times. The contemporaneous intrusion of the Pfarrberg augen gneiss (~ 271 Ma) represents the plutonic counterpart. To account for high-temperature magma generation and bimodal magmatism, we suggest an extensional (rift-related) environment that correlates well with regional considerations from the Eastern Alps and Western Carpathians.

In Triassic times, siliciclastic sediments (quartz arenite) followed by carbonate shelf sediments were deposited on top of the Troiseck Complex and the overlying volcanic rocks. The Troiseck-Floning Nappe formed during the Eo-Alpine collision, where it was part of the tectonic lower plate. A lower greenschist-facies metamorphic overprint that failed to obliterate pre-Alpine structures and geochronological data indicates subduction to only shallow crustal levels. Late Cretaceous exhumation of the Troiseck-Floning Nappe from

about 85 Ma onwards shows a gradient with more pronounced uplift and erosion in the eastern part.

Based on their analogous geological evolution, the Troiseck-Floning Nappe represents the eastern continuation of the Seckau Nappe. A similar type of basement occurs in parts of the Vorau Nappe (Chang et al., 2021; Neubauer et al., 2022) and in the Tatric and Veporic units of the Western Carpathians (e.g. Kohút et al., 2022). Altogether, the presented data closes a gap in the easternmost part of the Silvretta-Seckau Nappe System and provides new constraints for the correlation between the Eastern Alps and the Western Carpathians.

Supplementary Information

The online version contains supplementary material available at https://doi.org/10.1186/s00015-024-00456-5.

Additional file 1: Table S1. Analytical conditions for LA-ICP-MS zircon analyses.

Additional file 2: Table S2. U-Pb zircon data from analyzed samples and reference material. Analyses with discordance larger than 2% (marked in red) were discarded from further use.

Additional file 3: Table S3. Geochemical data.

Acknowledgements
For helpful discussions, we thank Axel Nowotny and Gerhard Bryda. Monika Horschinegg is acknowledged for her help performing the isotopic measurements. Furthermore, we would like to thank Stanislav Grabala for processing the samples and Andreas Wunderlich for preparing the thin sections. The authors are grateful for the comments and suggestions of Prof. Franz Neubauer and an anonymous reviewer, and for the editorial handling by Prof. Marko Vrabec and Dr. Daniel Marty.

Author contributions
MR, RS and JN conducted fieldwork in the Troiseck-Floning Nappe. CI prepared and analyzed zircon samples for U–Pb dating under the methodological supervision of DG. RS carried out Rb–Sr biotite analyses and edited the text. MR conceptualized and wrote the manuscript. All authors reviewed and approved the final manuscript.

Funding
Not applicable.

Availability of data and materials
The dataset supporting the conclusions of this article is included within the article and its additional files.

Declarations

Ethics approval and consent to participate
Not applicable.

Consent for publication
Not applicable.

Competing interests
The authors declare that they have no competing interests.

Author details
[1]Geosphere Austria, Hohe Warte 38, 1190 Vienna, Austria. [2]Institute of Earth Sciences, NAWI Graz Geocenter, University of Graz, Universitätsplatz 2/II, 8010 Graz, Austria. [3]Vienna, Austria.

Received: 30 June 2023 Accepted: 19 February 2024
Published online: 17 June 2024

References

Bachmann, O., & Bergantz, G. W. (2008). Rhyolites and their source mushes across tectonic settings. *Journal of Petrology, 49*(12), 2277–2285.

Ballèvre, M., Camonin, A., Manzotti, P., & Poujol, M. (2020). A step towards unraveling the paleogeographic attribution of pre-Mesozoic basement complexes in the Western Alps based on U-Pb geochronology of Permian magmatism. *Swiss Journal of Geosciences, 113*, 1–28.

Becker, L. (1980). Erläuterungen zu Blatt 162 Köflach. In *Geologische Karte der Republik Österreich 1:50.000* (p. 57), Wien: Geologische Bundesanstalt.

Bhatia, M. R., & Crook, K. A. (1986). Trace element characteristics of graywackes and tectonic setting discrimination of sedimentary basins. *Contributions to Mineralogy and Petrology, 92*(2), 181–193.

Bonin, B., Janoušek, V., & Moyen, J. F. (2020). Chemical variation, modal composition and classification of granitoids. *Geological Society, London, Special Publications, 491*(1), 9–51.

Broska, I., Janák, M., Svojtka, M., Yi, K., Konečný, P., Kubiš, M., Kurylo, S., Hrdlička, M., & Maraszewska, M. (2022). Variscan granitic magmatism in the Western Carpathians with linkage to slab break-off. *Lithos, 412*, 106589.

Bryda, G. Ćorić, S., van Husen, D., Kreuss, O., Mandl, G., Moser, M., Pavlik, W., Reiser, M. (2020). Blatt 102 Aflenz Kurort. In *Geologische Karte der Republik Österreich 1:50.000*. Wien: Geologische Bundesanstalt.

Burda, J., & Klötzli, U. (2011). Pre-Variscan evolution of the Western Tatra Mountains: New insights from U-Pb zircon dating. *Mineralogy and Petrology, 102*, 99–115.

Burda, J., Klötzli, U., Majka, J., Chew, D., Li, Q. L., Liu, Y., Gawęda, A., & Wiedenbeck, M. (2021). Tracing proto-Rheic-Qaidam Ocean vestiges into the Western Tatra mountains and implications for the Palaeozoic palaeogeography of Central Europe. *Gondwana Research, 91*, 188–204.

Catlos, E. J., Broska, I., Kohút, M., Etzel, T. M., Kyle, J. R., Stockli, D. F., Miggins, D. P., & Campos, D. (2022). Geochronology, geochemistry, and geodynamic evolution of Tatric granites from crystallization to exhumation (Tatra Mountains, Western Carpathians). *Geologica Carpathica, 73*(6), 517–544.

Chen, Y. X., Demény, A., Schertl, H. P., Zheng, Y. F., Huang, F., Zhou, K., Jin, Q.-Z., & Xia, X. P. (2020). Tracing subduction zone fluids with distinct Mg isotope compositions: Insights from high-pressure metasomatic rocks (leucophyllites) from the Eastern Alps. *Geochimica Et Cosmochimica Acta, 271*, 154–178.

Chang, R., Neubauer, F., Liu, Y., Yuan, S., Genser, J., Huang, Q., Guan, Q., & Yu, S. (2021). Hf isotopic constraints and detrital zircon ages for the Austroalpine basement evolution of Eastern Alps: Review and new data. *Earth-Science Reviews, 221*, 103772. https://doi.org/10.1016/j.earscirev.2021.103772

Chappell, B. W., & White, A. J. (2001). Two contrasting granite types: 25 years later. *Australian Journal of Earth Sciences, 48*(4), 489–499.

Cornelius, H. P. (1936). Mürzzuschlag 1:75.000. In *Geologische Spezialkarte der im Reichsrate vertretenen Königreiche und Länder der Österreich-Ungarischen Monarchie 1:75.000, Nr. 4955*. Wien: Geologische Bundesanstalt.

Cornelius, H. P. (1952). *Die Geologie des Mürztalgebietes (Erläuterungen zu Blatt Mürzzuschlag 1:75.000)*. Wien: Jahrbuch der Geologischen Bundesanstalt.

Dallmeyer, D. R., Neubauer, F., Handler, R., Fritz, H., Müller, W., Pană, D., & Putiš, M. (1996). Tectonothermal evolution of internal Alps and Carpathians: Evidence from $^{40}Ar/^{39}Ar$ mineral and whole-rock data. *Ecl. Geol. Helv., 89*, 203–227.

Dallmeyer, R. D., Handler, R., Neubauer, F., & Fritz, H. (1998). Sequence of thrusting within a thick-skinned tectonic wedge: Evidence from 40Ar/39Ar and Rb-Sr ages from the Austroalpine nappe complex of the Eastern Alps. *The Journal of Geology, 106*(1), 71–86.

Drummond, M. S., & Defant, M. J. (1990). A model for trondhjemite-tonalite-dacite genesis and crustal growth via slab melting: Archean to modern comparisons. *Journal of Geophysical Research: Solid Earth, 95*(B13), 21503–21521.

Faryad, S. W., Melcher, F., Hoinkes, G., Puhl, J., Meisel, T., & Frank, W. (2002). Relics of eclogite facies metamorphism in the Austroalpine basement, Hochgrossen (Speik complex), Austria. *Mineralogy and Petrology, 74*(1), 49–73.

Finger, F., & Riegler, G. (2023). The role of the proto-Alpine Cenerian Orogen in the Avalonian-Cadomian belt. *Austrian Journal of Earth Sciences, 116*(1), 109–115.

Fluegel, H. W., & Neubauer, F. (1984). Steiermark: Erläuterungen zur Geologischen Karte der Steiermark 1:200.000. In *Geologie der österreichischen Bundesländer in kurzgefassten Einzeldarstellungen* (p. 126). Wien: Geologische Bundesanstalt.

Foley, S., Tiepolo, M., & Vannucci, R. (2002). Growth of early continental crust controlled by melting of amphibolite in subduction zones. *Nature, 417*(6891), 837–840.

Froitzheim, N., Plašienka, D., & Schuster, R. (2008). Alpine tectonics of the Alps and Western Carpathians. In T. McCann (Ed.), *The geology of Central Europe volume 2: Mesozoic and Cenozoic*. Geological Society of London. https://doi.org/10.1144/CEV2P.6

Frost, B. R., Barnes, C. G., Collins, W. J., Arculus, R. J., Ellis, D. J., & Frost, C. D. (2001). A geochemical classification for granitic rocks. *Journal of Petrology, 42*(11), 2033–2048.

Frost, B. R., & Frost, C. D. (2008). A geochemical classification for feldspathic igneous rocks. *Journal of Petrology, 49*(11), 1955–1969.

Frost, C. D., & Frost, B. R. (2011). On ferroan (A-type) granitoids: Their compositional variability and modes of origin. *Journal of Petrology, 52*(1), 39–53.

Frost, C. D., Frost, B. R., & Beard, J. S. (2016). On silica-rich granitoids and their eruptive equivalents. *American Mineralogist, 101*(6), 1268–1284.

Gaal, G. (1965). Geologie des Roßkogelgebietes W Mürzzuschlag (Steiermark). *Mitteilungen der Gesellschaft Der Geologie- und Bergbaustudenten Österreichs, 16*, 105–148.

Gawęda, A., Burda, J., Klötzli, U., Golonka, J., & Szopa, K. (2016). Episodic construction of the Tatra granitoid intrusion (Central Western Carpathians, Poland/Slovakia): Consequences for the geodynamics of Variscan collision and Rheic Ocean closure. *International Journal of Earth Sciences, 105*, 1153–1174.

Glazner, A. F., Coleman, D. S., & Bartley, J. M. (2008). The tenuous connection between high-silica rhyolites and granodiorite plutons. *Geology, 36*(2), 183–186.

Haas, I., Eichinger, S., Haller, D., Fritz, H., Nievoll, J., Mandl, M., Hippler, D., & Hauzenberger, C. (2020). Gondwana fragments in the Eastern Alps: A travel story from U/Pb zircon data. *Gondwana Research, 77*, 204–222.

Handler, R. (1994). *40Ar/39Ar and Rb-Sr mineral dating within a complex polymetamorphic terrain: the northeastern Alps, Austria* (p. 143). Graz: Unpublished Dissertation Karl-Franzens-Universität.

Hastie, A. R., Kerr, A. C., Pearce, J. A., Mitchell, S. F. (2007). Classification of altered volcanic island arc rocks using immobile trace elements: development of the Th–Co discrimination diagram. *Journal of Petrology, 48*(12), 2341–2357. https://doi.org/10.1093/petrology/egm062

Hók, J., Schuster, R., Pelech, O., Vojtko, R., & Šamajová, L. (2022). Geological significance of upper Cretaceous sediments in deciphering of the Alpine tectonic evolution at the contact of the Western Carpathians, Eastern Alps and Bohemian Massif. *International Journal of Earth Sciences, 111*(6), 1805–1822.

Horstwood, M. S. A., Košler, J., Gehrels, G., Jackson, S. E., McLean, N. M., Paton, C., & Schoene, B. (2016). Community-derived standards for LA-ICP-MS U-(Th-)Pb geochronology—uncertainty propagation, age interpretation and data reporting. *Geostandards and Geoanalytical Research, 40*(3), 311–332. https://doi.org/10.1111/j.1751-908X.2016.00379.x

Huang, Q., Genser, J., Liu, Y., Neubauer, F., Yuan, S., Bernroider, M., Guan, Q., Jin, W., Yu, S., & Chang, R. (2021). Cambrian-Ordovician continental magmatic arc at the northern margin of Gondwana: Insights from the Schladming Complex, Eastern Alps. *Lithos*. https://doi.org/10.1016/j.lithos.2021.106064

Huang, Q., Neubauer, F., Liu, Y., Genser, J., Guan, Q., Chang, R., Yuan, S., & Yu, S. (2022). Permian-Triassic granites of the Schladming complex (Austroalpine basement): Implications for subduction of the Paleo-Tethys Ocean in the Eastern Alps. *Gondwana Research, 109*, 205–224.

Jackson, S. E., Pearson, N. J., Griffin, W. L., & Belousova, E. A. (2004). The application of laser ablation-inductively coupled plasma-mass spectrometry (LA-ICP-MS) to in-situ U-Pb zircon geochronology. *Chemical Geology, 211*(1–2), 47–69. https://doi.org/10.1016/j.chemgeo.2004.06.017

Janák, M., Plašienka, D., Frey, M., Cosca, M., Schmidt, S. T., Lupták, B., & Méres, Š. (2001). Cretaceous evolution of a metamorphic core complex, the Veporic unit, Western Carpathians (Slovakia): P-T conditions and in-situ $^{40}Ar/^{39}Ar$ UV laser probe dating of metapelites. *Journal of Metamorphic Geology, 19*(2), 197–216.

Janák, M., Petrík, I., Konečný, P., Kurylo, S., Kohút, M., & Madarás, J. (2022). Variscan metamorphism and partial melting of sillimanite-bearing metapelites in the High Tatra Mts. constrained by Th-U-Pb dating of monazite. *Geologica Carpathica, 73*(2), 97–122.

Janoušek, V., Farrow, C. M., & Erban, V. (2006). Interpretation of whole-rock geochemical data in igneous geochemistry: Introducing Geochemical Data Toolkit (GCDkit). *Journal of Petrology, 47*(6), 1255–1259.

Jeřábek, P., Lexa, O., Schulmann, K., & Plašienka, D. (2012). Inverse ductile thinning via lower crustal flow and fold-induced doming in the West Carpathian Eo-Alpine collisional wedge. *Tectonics*. https://doi.org/10.1029/2012TC003097

Knoll, T., Schuster, R., Huet, B., Mali, H., Onuk, P., Horschinegg, M., Ertl, A., & Giester, G. (2018). Spodumene pegmatites and related leucogranites from the Austroalpine Unit (eastern Alps, central Europe): Field relations, petrography, geochemistry, and geochronology. *The Canadian Mineralogist, 56*(4), 489–528.

Knoll, T., Huet, B., Schuster, R., Mali, H., Ntaflos, T., & Hauzenberger, C. (2023). Lithium pegmatite of anatectic origin—a case study from the Austroalpine Unit Pegmatite Province (Eastern European Alps): Geological data and geochemical modeling. *Ore Geology Reviews*. https://doi.org/10.1016/j.oregeorev.2023.105298

Kohút, M., & Larionov, A. N. (2021). From subduction to collision: Genesis of the Variscan granitic rocks from the Tatric Superunit (Western Carpathians, Slovakia). *Geologica Carpathica, 72*(2), 96–113.

Kohút, M., Linnemann, U., Hofmann, M., Gärtner, A., & Zieger, J. (2022). Provenance and detrital zircon study of the Tatric Unit basement (Western Carpathians, Slovakia). *International Journal of Earth Sciences, 111*(7), 2149–2168.

Králiková, S., Vojtko, R., Andriessen, P., Kováč, M., Fügenschuh, B., Hók, J., & Minár, J. (2014). Late Cretaceous-Cenozoic thermal evolution of the northern part of the Central Western Carpathians (Slovakia): Revealed by zircon and apatite fission track thermochronology. *Tectonophysics, 615*, 142–153.

Králiková, S., Vojtko, R., Hók, J., Fügenschuh, B., & Kováč, M. (2016). Low-temperature constraints on the Alpine thermal evolution of the Western Carpathian basement rock complexes. *Journal of Structural Geology, 91*, 144–160.

Kristan-Tollmann, E., & Tollmann, A. (1967). Crinoiden aus dem zentralalpinen Anis (Leithagebirge, Thörler Zug und Radstädter Tauern). In *Wissenschaftliche Arbeiten aus dem Burgenland (WAB), Nr.* 36, (pp. 28–33). Eisenstadt: Landesmuseum Burgenland.

Laurent, A., Janoušek, V., Magna, T., Schulmann, K., & Míková, J. (2014). Petrogenesis and geochronology of a post-orogenic calc-alkaline magmatic association: The Zulova Pluton, Bohemian Massif. *Journal of Geosciences, 59*(4), 415–440.

Linnemann, U., Gerdes, A., Hofmann, M., & Marko, L. (2014). The Cadomian Orogen: Neoproterozoic to Early Cambrian crustal growth and orogenic zoning along the periphery of the West African Craton—Constraints from U-Pb zircon ages and Hf isotopes (Schwarzburg Antiform, Germany). *Precambrian Research, 244*, 236–278.

Mandl, M., Kurz, W., Hauzenberger, C., Fritz, H., Klötzli, U., & Schuster, R. (2018). Pre-Alpine evolution of the Seckau Complex (Austroalpine basement/Eastern Alps): Constraints from in-situ LA-ICP-MS U-Pb zircon geochronology. *Lithos, 296*, 412–430.

Mandl, M., Kurz, W., Hauzenberger, C., Fritz, H., & Pfingstl, S. (2022). Geochemistry of granitoids from the Austroalpine Seckau Complex: A key for revealing the pre-Alpine evolution of the Eastern Alps. *Mineralogy and Petrology, 116*(3), 251–272.

McDonough, W. F., & Sun, S. S. (1995). The composition of the Earth. *Chemical Geology, 120*(3–4), 223–253.

McLennan, S. M. (2001). Relationships between the trace element composition of sedimentary rocks and upper continental crust. *Geochemistry, Geophysics, Geosystems*. https://doi.org/10.1029/2000GC000109
Melcher, F., & Meisel, T. (2004). A metamorphosed Early Cambrian crust–mantle transition in the Eastern Alps, Austria. *Journal of Petrology, 45*(8), 1689–1723.
Meschede, M. (1986). A method of discriminating between different types of mid-ocean ridge basalts and continental tholeiites with the Nb-Zr-Y diagram. *Chemical Geology, 56*(3–4), 207–218.
Middlemost, E. A. (1994). Naming materials in the magma/igneous rock system. *Earth-Science Reviews, 37*(3–4), 215–224.
Moussallam, Y., Schneider, D. A., Janák, M., Thöni, M., & Holm, D. K. (2012). Heterogeneous extrusion and exhumation of deep-crustal Variscan assembly: Geochronology of the Western Tatra Mountains, northern Slovakia. *Lithos, 144*, 88–108.
Moyen, J. F., & Martin, H. (2012). Forty years of TTG research. *Lithos, 148*, 312–336.
Neubauer, F. (1988). Structural evolution of the Rennfeld-Mugel area and Gleinalm crystalline complex (Eastern Alps). *Abhandlungen der Geologischen Bundesanstalt, 42*, 5–137.
Neubauer, F., Handler, R., Hermann, S., & Paulus, G. (1994). Revised Lithostratigraphy and Structure of the Eastern Graywacke Zone (Eastern Alps). *Mitteilungen Österreichische Geologische Gesellschaft, 86*, 61–74.
Neubauer, F., Dallmeyer, R. D., Dunkl, I., & Schirnik, D. (1995). Late cretaceous exhumation of the metamorphic Gleinalm dome, Eastern Alps: kinematics, cooling history and sedimentary response in a sinistral wrench corridor. *Tectonophysics*, *242*(1–2), 79–98. https://doi.org/10.1016/0040-1951(94)00154-2
Neubauer, F., Frisch, W., & Hansen, B. T. (2003). Early Paleozoic and Variscan events in the Austroalpine Rennfeld block (Eastern Alps): A U-Pb study. *Jahrbuch der Geologischen Bundesanstalt, 143*, 567–580.
Neubauer, F., Liu, Y., Chang, R., Yuan, S., Yu, S., Genser, J., Liu, B., & Guan, Q. (2020). The Wechsel Gneiss Complex of Eastern Alps: An Ediacaran to Cambrian continental arc and its Early Proterozoic hinterland. *Swiss Journal of Geosciences, 113*(1), 1–23.
Neubauer, F., Liu, Y., Dong, Y., Chang, R., Genser, J., & Yuan, S. (2022). Pre-Alpine tectonic evolution of the Eastern Alps: From prototethys to paleotethys. *Earth-Science Reviews, 226*, 103923.
Nievoll, J. (1985). Die bruchhafte Tektonik entlang der Trofaiachlinie (Östliche Zentralalpen, Österreich). *Jahrbuch der Geologischen Bundesanstalt, 127*, 643–671.
Nievoll, J. (1986). Bericht 1985 über geologische Aufnahmen auf Blatt 103 Kindberg. *Jahrbuch der Geologischen Bundesanstalt, 129*(2), 409–411.
O'Connor, J. T. (1965). A classification for quartz-rich igneous rocks based on feldspar ratios. *US Geological Survey, Professional Papers, 525B*, B79–B84.
Ondrejka, M., Uher, P., Putiš, M., Kohút, M., Broska, I., Larionov, A., Bojar, A.-V., & Sobocký, T. (2021). Permian A-type granites of the Western Carpathians and Transdanubian regions: Products of the Pangea supercontinent breakup. *International Journal of Earth Sciences, 110*(6), 2133–2155.
Paton, C., Woodhead, J. D., Hellstrom, J. C., Hergt, J. M., Greig, A., & Maas, R. (2010). Improved laser ablation U-Pb zircon geochronology through robust downhole fractionation correction. *Geochemistry, Geophysics, Geosystems*. https://doi.org/10.1029/2009GC002618
Paton, C., Hellstrom, J., Paul, B., Woodhead, J., & Hergt, J. (2011). Iolite: Freeware for the visualisation and processing of mass spectrometric data. *Journal of Analytical Atomic Spectrometry, 26*(12), 2508–2518.
Pearce, J. A., Harris, N. B., & Tindle, A. G. (1984). Trace element discrimination diagrams for the tectonic interpretation of granitic rocks. *Journal of Petrology, 25*(4), 956–983.
Pearce, J. (1996). Sources and settings of granitic rocks. *Episodes, 19*(4), 120–125. https://doi.org/10.18814/epiiugs/1996/v19i4/005
Petrik, I., Janák, M., Vaculovič, T., Konečný, P., & Méres, Š. (2020). Variscan high-pressure metamorphism of kyanite-bearing paragneisses hosting eclogites in the Veporic unit, Western Carpathians: Evidence from Th–U–Pb dating of monazite. *Geologica Carpathica, 71*(6), 485–502. https://doi.org/10.31577/GeolCarp.71.6.1
Pfingstl, S., Kurz, W., Schuster, R., & Hauzenberger, C. (2015). Geochronological constraints on the exhumation of the Austroalpine Seckau Nappe (Eastern Alps). *Austrian Journal of Earth Sciences, 108*(1), 172–185.
Plašienka, D. (2018). Continuity and episodicity in the early Alpine tectonic evolution of the Western Carpathians: How large-scale processes are expressed by the orogenic architecture and rock record data. *Tectonics, 37*(7), 2029–2079.
Putiš, M., Ivan, P., Kohút, M., Spišiak, J., Siman, P., Radvanec, M., Uher, P., & Ondrejka, M. (2009a). Meta-igneous rocks of the West-Carpathian basement, Slovakia: Indicators of Early Paleozoic extension and shortening events. *Bulletin de la Société Géologique de France, 180*(6), 461–471.
Putiš, M., Frank, W., Plašienka, D., Siman, P., Sulák, M., & Biron, A. (2009b). Progradation of the Alpidic Central Western Carpathians orogenic wedge related to two subductions: Constrained by 40Ar/39Ar ages of white micas. *Geodinamica Acta, 22*(1–3), 31–56.
Putiš, M., Li, J., Ružička, P., Ling, X., & Nemec, O. (2016). U/Pb SIMS zircon dating of a rhyolite intercalation in Permian siliciclastics as well as a rhyodacite dyke in micaschists (Infratatricum, W. Carpathians). *Mineralia Slovaca, 48*(2), 135–144.
Rantitsch, G., Bryda, G., & Gawlick, H. J. (2020). Conodont thermometry by Raman spectroscopy on carbonaceous material: A case study from the Northern Calcareous Alps (Mürzalpen Nappe, Eastern Alps). *Austrian Journal of Earth Sciences, 113*(2), 201–210.
Rapp, R. P., Watson, E. B., & Miller, C. F. (1991). Partial melting of amphibolite/eclogite and the origin of Archaean trondhjemites and tonalites. *Precambrian Research, 51*, 1–25.
Reiser, M. (2020). Bericht 2019 über strukturgeologische Aufnahmen in der Troiseck-Floning-Decke auf Blatt 102 Aflenz Kurort. *Jahrbuch der Geologischen Bundesanstalt, 160*, 458–460.
Scharbert, S. (1981). Untersuchungen zum Alter des Seckauer Kristallins. *Mitteilungen der Gesellschaft der Geologie- und Bergbaustudenten Österreichs, 27*, 173–188.
Schermaier, A., Haunschmid, B., & Finger, F. (1997). Distribution of Variscan I- and S-type granites in the Eastern Alps: A possible clue to unravel pre-Alpine basement structures. *Tectonophysics, 272*(2–4), 315–333.
Schmid, S. M., Fügenschuh, B., Kissling, E., & Schuster, R. (2004). Tectonic map and overall architecture of the Alpine orogen. *Eclogae Geologicae Helvetiae, 97*, 93–117.
Schmidt, K. (1999). Geochronologie entlang eines Metamorphoseprofils vom S-Rand der Nördlichen Kalkalpen bis zum Unterostalpin des Semmeringgebietes (Niederösterreich, Steiermark).—Unpublished Diploma Thesis (p. 127). Wien: University of Vienna.
Schuster, R., Scharbert, S., Abart, R., & Frank, W. (2001). Permo-Triassic extension and related HT/LP metamorphism in the Austroalpine-Southalpine realm. *Mitteilungen der Gesellschaft der Geologie- und Bergbaustudenten Österreichs, 44*, 111–141.
Schuster, R., & Stüwe, K. (2008). Permian metamorphic event in the Alps. *Geology, 36*(8), 603–606.
Schuster, R., & Nowotny, A. (2016). Die Einheiten des Ostalpinen Kristallins auf den Kartenblättern GK50 Blatt 103 Kindberg und 135 Birkfeld. In *Arbeitstagung der Geologischen Bundesanstalt Geologie der Kartenblätter GK50 ÖK 103 Kindberg und ÖK 135 Birkfeld, Mitterdorf im Mürztal 21.-25. September 2015* (pp. 10–37). Wien: Geologische Bundesanstalt.
Schuster, R. (2016). Grauwackenzone und Veitsch-Silbersberg-Deckensystem. In *Arbeitstagung der Geologischen Bundesanstalt Geologie der Kartenblätter GK50 ÖK 103 Kindberg und ÖK 135 Birkfeld, Mitterdorf im Mürztal 21.-25. September 2015* (pp. 38–43). Wien: Geologische Bundesanstalt.
Siegesmund, S., Oriolo, S., Heinrichs, T., Basei, M. A. S., Nolte, N., Hüttenrauch, F., & Schulz, B. (2018). Provenance of Austroalpine basement metasediments: Tightening up Early Palaeozoic connections between peri-Gondwanan domains of central Europe and Northern Africa. *International Journal of Earth Sciences, 107*, 2293–2315.
Siegesmund, S., Oriolo, S., Schulz, B., Heinrichs, T., Basei, M. A. S., & Lammerer, B. (2021). The birth of the Alps: Ediacaran to Paleozoic accretionary processes and crustal growth along the northern Gondwana margin. *International Journal of Earth Sciences, 110*(4), 1321–1348.
Siegesmund, S., Oriolo, S., Broge, A., Hueck, M., Lammerer, B., Basei, M. A., & Schulz, B. (2023). Cadomian to Cenerian accretionary orogenic processes in the Alpine basement: the detrital zircon archive. *International Journal of Earth Sciences*. https://doi.org/10.1007/s00531-023-02305-6
Sláma, J., Košler, J., & Pedersen, R. B. (2007). Behaviour of zircon in high-grade metamorphic rocks: Evidence from Hf isotopes, trace elements and textural studies. *Contributions to Mineralogy and Petrology, 154*, 335–356.
Sölva, H., Grasemann, B., Thöni, M., Thiede, R., & Habler, G. (2005). The Schneeberg normal fault zone: Normal faulting associated with Cretaceous

SE-directed extrusion in the Eastern Alps (Italy/Austria). *Tectonophysics, 401*(3–4), 143–166.
Spengler, E. (1921). Zur Tektonik des obersteirischen Karbonzuges bei Thörl und Turnau. *Jahrbuch Der Geologischen Reichsanstalt, 70*, 235–254.
Stephan, T., Kroner, U. W. E., & Romer, R. L. (2019a). The pre-orogenic detrital zircon record of the Peri-Gondwanan crust. *Geological Magazine, 156*(2), 281–307.
Stephan, T., Kroner, U., Romer, R. L., & Rösel, D. (2019b). From a bipartite Gondwanan shelf to an arcuate Variscan belt: The early Paleozoic evolution of northern Peri-Gondwana. *Earth-Science Reviews, 192*, 491–512.
Tari, G., Bada, G., Beidinger, A., Csizmeg, J., Danišik, M., Gjerazi, I., Grasemann, B., Kováč, M., Plašienka, D., Šujan, M., & Szafián, P. (2021). The connection between the Alps and the Carpathians beneath the Pannonian Basin: Selective reactivation of Alpine nappe contacts during Miocene extension. *Global and Planetary Change, 197*, 103401.
Tollmann, A. (1977). *Geologie von Österreich: Die Zentralalpen* (Vol. 1, p. 766). Franz Deuticke Verlag.
Thöni, M., & Miller, C. (2000). Permo-Triassic pegmatites in the eo-Alpine eclogite-facies Koralpe complex, Austria: Age and magma source constraints from mineral chemical, Rb-Sr and Sm-Nd isotope data. *Schweizerische Mineralogische Und Petrographische Mitteilungen, 80*(2), 169–186.
Thöni, M. (2006). Dating eclogite-facies metamorphism in the Eastern Alps–approaches, results, interpretations: A review. *Mineralogy and Petrology, 88*, 123–148.
Thöni, M., & Miller, C. (2009). The "Permian event" in the Eastern European Alps: Sm–Nd and P-T data recorded by multi-stage garnet from the Plankogel unit. *Chemical Geology, 260*(1–2), 20–36.
Uher, P., Broska, I., Krzemińska, E., Ondrejka, M., Mikuš, T., & Vaculovič, T. (2019). Titanite composition and SHRIMP U-Pb dating as indicators of post-magmatic tectono-thermal activity: Variscan I-type tonalites to granodiorites, the Western Carpathians. *Geologica Carpathica, 70*(6), 449–470.
van Gelder, I. E., Willingshofer, E., Andriessen, P. A. M., Schuster, R., & Sokoutis, D. (2020). Cooling and vertical motions of crustal wedges prior to, during and after lateral extrusion in the Eastern Alps: New fieldkinematic and fission track data from the Mur-Mürz fault system. *Tectonics*. https://doi.org/10.1029/2019TC005754
Vermeesch, P. (2018). IsoplotR: A free and open toolbox for geochronology. *Geoscience Frontiers, 9*(5), 1479–1493.
Vermeesch, P. (2021). Maximum depositional age estimation revisited. *Geoscience Frontiers, 12*(2), 843–850.
Veselá, P., Lammerer, B., Wetzel, A., Söllner, F., & Gerdes, A. (2008). Post-Variscan to Early Alpine sedimentary basins in the Tauern window (eastern Alps). *Geological Society, London, Special Publications, 298*(1), 83–100.
Villaseñor, G., Catlos, E. J., Broska, I., Kohút, M., Hraško, Ľ, Aguilera, K., Etzel, T. M., Kyle, J. R., & Stockli, D. F. (2021). Evidence for widespread mid-Permian magmatic activity related to rifting following the Variscan orogeny (Western Carpathians). *Lithos, 390*, 106083.
Visonà, D., Fioretti, A. M., Poli, M. E., Zanferrari, A., & Fanning, M. (2007). U-Pb SHRIMP zircon dating of andesite from the Dolomite area (NE Italy): Geochronological evidence for the early onset of Permian Volcanism in the eastern part of the Southern Alps. *Swiss Journal of Geosciences, 100*(2), 313–324.
Vojtko, R., Králiková, S., Jeřábek, P., Schuster, R., Danišík, M., Fügenschuh, B., Minár, J., & Madarás, J. (2016). Geochronological evidence for the Alpine tectono-thermal evolution of the Veporic Unit (Western Carpathians, Slovakia). *Tectonophysics, 666*, 48–65.
Vozárová, A., Šarinová, K., Rodionov, N., & Vozar, J. (2020). Zircon U-Pb geochronology from Permian rocks of the Tribeč Mts.(Western Carpathians, Slovakia). *Geologica Carpathica, 71*(3), 274–287.
von Raumer, J. F., & Stampfli, G. M. (2008). The birth of the Rheic ocean—early Palaeozoic subsidence patterns and subsequent tectonic plate scenarios. *Tectonophysics, 461*(1–4), 9–20.
Whalen, J.B., Currie, K.L. & Chappell, B.W. (1987). A-type granites: geochemical characteristics, discrimination and petrogenesis. *Contributions to Mineralogy and Petrology*, *95*, 407–419. https://doi.org/10.1007/BF00402202
Whitney, D. L., & Evans, B. W. (2010). Abbreviations for names of rock-forming minerals. *American Mineralogist, 95*(1), 185–187.
Winchester, J. A., & Floyd, P. A. (1977). Geochemical discrimination of different magma series and their differentiation products using immobile elements. *Chemical Geology, 20*, 325–343.
Yuan, S., Neubauer, F., Liu, Y., Genser, J., Liu, B., Yu, S., Chang, R. & Guan, Q. (2020). Widespread Permian granite magmatism in Lower Austroalpine units: significance for Permian rifting in the Eastern Alps. *Swiss Journal of Geosciences*, 113(18). https://doi.org/10.1186/s00015-020-00371-5.
Zurbriggen, R. (2017). The Cenerian orogeny (early Paleozoic) from the perspective of the Alpine region. *International Journal of Earth Sciences, 106*(2), 517–529.
Zurbriggen, R. (2020). Banded amphibolites in the Alps: A new interpretation in relation to early Paleozoic peraluminous magmatism. *Swiss Journal of Geosciences, 113*(1), 1–24.

Publisher's Note